Gradstein F. M., Ludden, J. N., et al., 1992
Proceedings of the Ocean Drilling Program, Scientific Results, Vol. 123

8. GEOCHEMISTRY OF SEDIMENTS IN THE ARGO ABYSSAL PLAIN AT SITE 765: A CONTINENTAL MARGIN REFERENCE SECTION FOR SEDIMENT RECYCLING IN SUBDUCTION ZONES[1]

Terry Plank[2] and John N. Ludden[3]

ABSTRACT

Drilling at Site 765 in the Argo Abyssal Plain sampled sediments and oceanic crust adjacent to the Australian margin. Some day, this site will be consumed in the Java Trench. An intensive analytical program was conducted to establish this site as a geochemical reference section for crustal recycling calculations. About 150 sediment samples from Site 765 were analyzed for major and trace elements. Downhole trends in the sediment analyses agree well with trends in sediment mineralogy, as well as in Al and K logs. The primary signal in the geochemical variability is dilution of a detrital component by both biogenic silica and calcium carbonate. Although significant variations in the nonbiogenic component occur through time, its overall character is similar to nearby Canning Basin shales, which are typical of average post-Archean Australian shales (PAAS). The bulk composition of the hole is calculated using core descriptions to weight the analyses appropriately. However, a remarkably accurate estimate of the bulk composition of the hole can be made simply from PAAS and the average calcium carbonate and aluminum contents of the hole. Most elements can be estimated within 30% in this way. This means that estimating the bulk composition of other sections dominated by detrital and biogenic components may require little analytical effort: calcium carbonate contents, average Al contents, and average shale values can be taken from core descriptions, geochemical logs, and the literature, respectively. Some of the geochemical systematics developed at Site 765 can be extrapolated along the entire Sunda Trench. However, results are general, and Site 765 should serve as a useful reference for estimating the compositions of other continental margin sections approaching trenches around the world (e.g., outboard of the Lesser Antilles, Aegean, and Eolian arcs).

INTRODUCTION

The extent to which the continental crust is recycled back into the mantle via sediment subduction is crucial to our understanding of how Earth's mantle and crust evolved. Primarily, two lines of evidence support sediment subduction. One is based on seismic surveys and drilling that show an absence of accreted sediments in some forearcs (e.g., in the Marianas: Hussong, Uyeda, et al., 1982; Guatemala: Moore, Backman, et al., 1982; and Peru: Warsi et al., 1983). Even where well-developed accretionary wedges occur, often evidence indicates that some sediment is also being subducted beneath décollement structures in the wedge (as in the Lesser Antilles: Westbrook et al., 1988) or in grabens developed in the bending plate (as for the Nazca Plate approaching the Peru-Chile Trench: Schweller et al., 1981). Thus, ample geophysical evidence exists to show that sediment is subducted, at least beneath some forearcs.

A second line of evidence for sediment subduction comes from the isotope ^{10}Be. An isotope strongly enriched in soils and marine clays, ^{10}Be is found in measurable quantities in arc volcanics, but not in volcanics from other tectonic settings (Tera et al., 1986). This means that some surface sediments are taken as far as the site of arc magma genesis (~120 km deep). The factors that lead to sediment subduction in some situations, and not others, are still poorly understood (a modern twist on an old soliloquy provides a recent discussion of the various models; Von Huene, 1986).

The issue of *how much* sediment gets subducted to great depths remains open. Arc magmas incorporate some quantity of sediment and provide our best means for estimating the fluxes involved. However, these calculations require knowledge of the geochemical characteristics of both the influx (sediment and crust approaching trenches) and the output (arc volcanics). Although a fairly comprehensive global data base exists of the geochemical composition of arc volcanics, a method has yet to be developed for estimating the composition of the diverse sediment sections approaching trenches. A considerable amount of geochemical data exist for marine sediments. Most chemical analyses of sediments, however, consist of a few elements specific to oceanographic problems, and not necessarily solid earth ones. These data provide a first-order understanding of the systematics of sediment compositions, but do not constrain well what compositions are appropriate for individual subduction zones. Estimates of sediment compositions outboard of trenches usually are based on analyses of a few surface sediments, whole-ocean averages, or average "pelagic sediment." These estimates need to be refined. For example, elements that are used as tracers for sediment influxes to arc magma sources (e.g., K_2O; Karig and Kay, 1980) may vary considerably in "pelagic sediments," on the order of all igneous rocks on the face of Earth. This is because sediments represent mixtures of biogenic carbonate or silica, which are devoid of most trace elements, and continental detritus or Fe-Mn oxides, which are rich in many trace metals. Thus, although ratios of certain elements and isotopic compositions of sediments are fairly well constrained, the actual element abundances may vary enormously. Ultimately, it is concentration data, not element or isotopic ratios, that are necessary for answering the question of *how much*?

Here, we discuss the geochemistry of the sedimentary section of Site 765, drilled during Leg 123 in the Argo Abyssal Plain, south of Java. These sediments may someday be consumed in the Sunda Trench. Full characterization of potential crustal fluxes into the Sunda Trench should include other sedimentary components that may be added to Site 765 as it drifts northward: volcanic ash derived from the arc itself and clastic material derived from

[1] Gradstein, F. M., Ludden, J. N., et al., 1992. *Proc. ODP, Sci. Results,* 123: College Station, TX (Ocean Drilling Program).
[2] Lamont-Doherty Geological Observatory and Department of Geological Sciences of Columbia University, Palisades, NY 10964, U.S.A.
[3] Département de Géologie, Université de Montréal, C.P. 6128 Succ. A, Montréal, Québec, H3C 3J7, Canada.

the Ganges-Brahmaputra river system via the Nicobar Fan. In addition to sedimentary components, the chemical additions to the basaltic substrate via seawater alteration constitutes another crustal component. Gillis et al. (this volume) present some preliminary conclusions regarding the geochemical fluxes involved during alteration of the basaltic crust at Site 765.

Although the data presented here have obvious bearing on problems specific to the Sunda Arc as well as to the sedimentological history of the Australian margin, the thrust of this study is more general: to provide a reference data set for sediment subduction globally. Indeed, Site 765 represents an end-member of sorts. The site is situated adjacent to a passive margin, and so represents the crust first formed when an ocean basin opens, and the last consumed when an ocean basin disappears down a subduction zone. The sediments that have accumulated at Site 765 are dominated by detrital material derived from the Australian continent. Thus, Site 765 should serve as a reference site for other subduction zones proximal to continental sediment sources (e.g., the Lesser Antilles, the American, and the Eolian/Aegean arcs). We hope to provide here a methodology for constraining sediment influx to this class of subduction zones, and in doing so, to begin to answer the question of *how much?*

First, we present a geochemical stratigraphy of Site 765 sediments, attempt to tie the geochemical variability to the lithologic variability, and briefly speculate about the provenance of the sediments. Next, we devise a method for estimating the bulk composition of the entire sediment section. Finally, we discuss the relevance of this site to sedimentary sections globally, as well as regionally along the Sunda Arc.

GEOLOGIC BACKGROUND

Site 765 is situated in the Argo Abyssal Plain, a triangular region of some of the oldest crust of the Indian Ocean, sandwiched between the northwestern margin of Australia and the Java Trench (see Fig. 1). The crust drilled at Site 765 represents the first oceanic crust formed during rifting of the Australian margin in the Earliest Cretaceous. This site is now only 500 km away from being consumed at the Sunda Trench, south of Java. The sedimentary section that has accumulated is thin for a passive margin sequence owing to the arid climate and low relief of western Australia. Although several active and explosive volcanoes are located on Java and the Lesser Sunda Islands, Site 765 has yet to enter the region of extensive ash falls determined by Ninkovich (1979). Thus, the ultimate source of much of the sediment at Site 765 is the Pilbara and Kimberly blocks of northwestern Australia craton, which are Archean to Proterozoic in age (Fig. 1). Although Site 765 is at abyssal depths, sedimentation rates have been higher than typical abyssal rates (see Ludden, Gradstein, et al., 1990), especially during the Neogene (averaging 27 m/m.y.) due to the continual supply of material from the Australian Shelf and Exmouth Plateau via turbidity flows. Even though well below the calcite compensation depth, the hole has a high carbonate content owing to the rapid influx and burial of pelagic carbonates from the Australian margin.

At Site 765, roughly 950 m of sediment was cored above the basaltic basement. The sedimentary section can be divided in two, corresponding grossly to the Cenozoic and Cretaceous sections. The Cenozoic section is dominated by calcareous turbidites, prob-

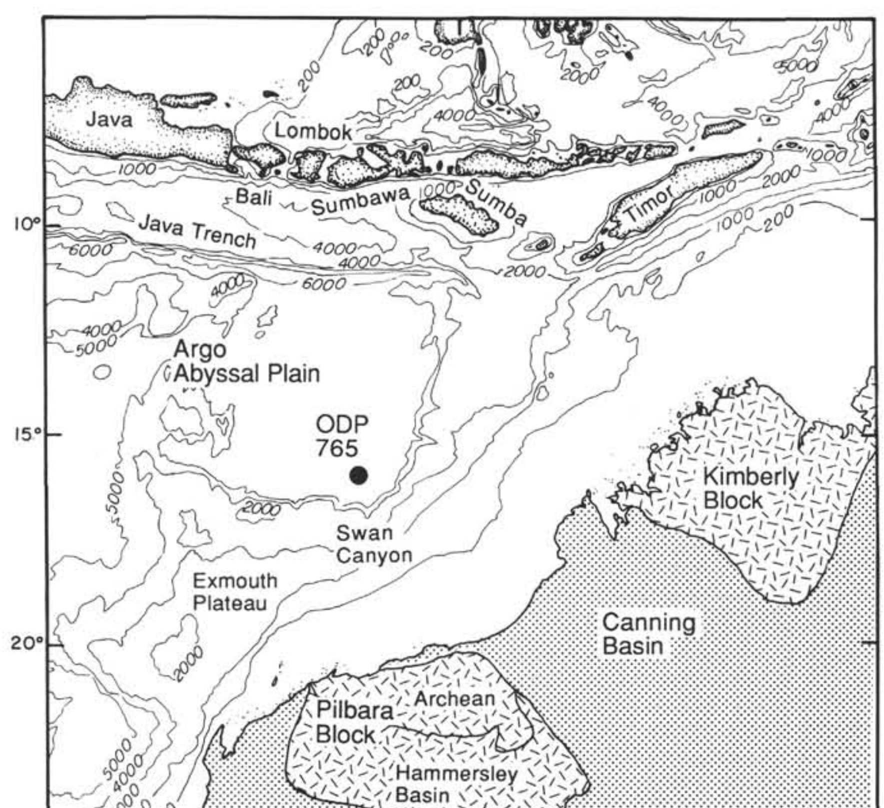

Figure 1. Location map of Site 765 with simplified geology of northwestern Australia. Water depth contours in meters.

ably originating on the Exmouth Plateau and fed by the Swan Canyon (Fig. 1). Although calcareous sequences also occur throughout the Cretaceous section, this lower section is dominated by pelagic clays. Within this simple division, however, tremendous lithologic diversity is represented by foraminiferal sands, nannofossil oozes, radiolarites, Mn-rich horizons, and red, green, and black clays.

SAMPLING AND ANALYTICAL DETAILS

Our sampling strategy was to take one 40-cm^3 sample at each core that was representative of a dominant lithology in that core. Thus, we have a fairly evenly spaced sampling every 10 m or so down the entire 930-m section. Some sections of cores were subsampled (three individual turbidite units and red and green clay units in the lower half of the hole), and several samples were taken in adjacent intervals to assess variability at the centimeter scale. Samples were powdered and homogenized by first baking to 110°C, then pulverizing in either a tungsten carbide shatterbox or an alumina ball-mill.

About 70 samples were analyzed on board the *Resolution* using X-ray fluorescence (XRF) for all the major elements and for Rb, Sr, Ba, Y, Zr, Nb, V, Cr, Ni, Cu, and Zn (Table 1). Another 70 samples were analyzed at Lamont-Doherty (LDGO) by direct-current plasma emission spectrometry (DCP) for all the major elements and for Sr, Ba, Y, Zr, V, Cr, Ni, Cu, Zn, and Sc (Table 1). Forty samples were selected for additional instrumental neutron activation analysis (INAA) at the Université de Montréal, for REE, U, Th, Sc, Cr, Hf, Ta, W, Co, As, Sb, Ba, and Cs (Table 2). The major- and trace-element analyses for these same samples or for adjacent intervals are presented in Table 1. Details of the XRF and INAA procedures are given in Ludden, Gradstein, et al. (1990) and in Francis and Ludden (1990), respectively. Analysis of sediment samples by DCP required new procedures, which are described below.

Different routines were set up for running clay- and carbonate-rich samples by DCP. The clay-rich samples (with 10% CaO) proved as straightforward to analyze as igneous rocks, and procedures were followed similar to those outlined in Klein et al. (1991). For each batch of clay samples (usually 10 unknowns), the USGS standards SCO-1 and QLO, as well as an in-house Aleutian andesite standard, LUM-37, were used to establish the calibration curves.

The analysis of carbonate-rich samples (>10% CaO) required some modifications to our routine method. Preliminary shipboard work revealed a problem in alkali loss upon ignition. We overcame this problem on board the ship by analyzing the alkali elements (K, Na, and Rb) on unignited powder pellets, although these measurements are inherently less accurate for K and Na, which are normally analyzed on fused glass disks. A new procedure had to be developed for the DCP method as well, because samples typically are fused and dissolved after ignition. However, comparison with analyses by total HF-$HClO_4$ dissolution indicated that alkali loss occurred only during ignition of samples (30 min at 1000°C), not during $LiBO_2$ fusion. In the most carbonate-rich samples, some K was lost during the standard 15-min fusion at 1050°C; times were then reduced to 5 min, which seemed sufficient for fusion without alkali loss. Thus, carbonate samples were fused and dissolved without first oxidizing or devolatilizing. Total volatile loss on ignition (LOI) was determined for separate splits.

Significant Ca interferences or enhancements occurred on the Al line and on all the trace-element lines of our multi-element cassettes (the specific wavelengths used for each element are available upon request). With the exceptions of Sc, Y, and Zr, however, the Ca interferences are linear and easily corrected by running a pure CaO standard during each run. Calibration curves for each batch of unknowns were constructed using pure CaO, LUM-37, and mixtures of the two in the proportions 1:1 and 1:3. These CaO-andesite mixtures provided us both with standards that closely resembled the unknowns and with dependable values for the trace elements, which is important because few well-characterized carbonate standards exist. Sc, Y, and Zr have large Ca interferences and are matrix sensitive (Ca enhances and Si suppresses). As a consequence, the standards do not form good calibration curves, and the Sc, Y, and Zr data are not accurate (10%–20% relative). More recent tests have shown that matrix problems are reduced by using a factor of 2 greater dilution (1:500) and a greater flux to sample ratio (10:1). With this procedure, standards form acceptable lines, and thus the Sc, Y, and Zr data are more accurate (5%), but because of the greater dilution, the peak-to-background ratios suffer, and the data are less precise (10%).

XRF analyses were presented in Ludden, Gradstein, et al. (1990), but have been reproduced here (Table 1) because an additional normalization factor was applied. In addition, K_2O was re-run for the powder pellets by XRF at the Université de Montréal, and these newer analyses are reported here. On board the ship, the standard SCO-1 was run with every batch of samples; the precision based on these replicates is good (generally better than 2% relative for the major elements and 4% for the trace elements; see Table 21 in Ludden, Gradstein, et al., 1990). The DCP data are similarly precise, based on analysis of an Indian Ocean brown clay sample (IOBC) that was used to monitor drift during 10 different runs (Table 3). The Na_2O and MnO values determined by DCP are more precise than the XRF determinations, while the Zr and Y XRF values are preferred because of the matrix problems with the DCP mentioned above.

Although both methods are precise, the agreement between the two varies for different elements. Powders analyzed using both XRF and DCP show consistent discrepancies. These differences are almost always of the same direction and magnitude as the differences between the accepted values for SCO-1 (Govindaraju, 1989) and those determined by XRF. Thus, normalization factors were applied to the XRF data based on the DCP duplicates and the accepted SCO-1 values (see Table 3 for the original XRF average for SCO-1, the Govindaraju values, and the values after normalization). The XRF Ce values and the DCP Sc values were also adjusted to agree with the more precise INAA values. Thus, the data presented in Table 1 show minimal analytical biases (all elements generally agree among methods to 5% relative).

Analyses of adjacent samples, where one was powdered in the ball mill and one was powdered in the shatterbox, indicate contamination of a few elements by the tungsten carbide shatterbox (2–4 ppm Co, 0.3–0.4 ppm Ta, and 35–60 ppm W). Aluminum contamination caused by powdering in the alumina ball mill, however, was negligible. The powdering method is listed along with the INAA analyses in Table 2.

GEOCHEMICAL VARIABILITY

The simplest way to estimate the bulk composition of a sedimentary section might be to sample continuously down the core, analyze the samples, and then average them. This is impractical for a section that is almost 1 km long, such as was cored at Site 765. This is certainly an impractical method for estimating the flux of material entering oceanic trenches globally. Because our sampling and analytical efforts were intensive for Site 765, we can estimate fairly accurately its bulk composition simply by averaging the analyses reported in Tables 1 and 2. However, our aim was not only to calculate the bulk composition of Site 765 sediments, but also to develop a less analytically intensive method for estimating sections elsewhere. One advantage to working with DSDP/ODP cores is the wealth of lithological and mineralogical

Table 1. Analyses of major and trace elements in Site 765 sediments.

123-765B	1H-4, 48-50	2H-3, 94-106	2H-3, 123-135	2H-3, 145-150	2H-4, 7-19	2H-4, 31-43	2H-4, 91-103	2H-4, 131-143	2H-6, 138-140	2H-6, 140-142
Depth:	4.98	13.24	13.53	13.75	13.87	14.11	14.71	15.11	18.18	18.20
Color:	Lt ol gray	Lt ol gray	Ol gray	Ol gray	Ol gray	Lt olive	Lt olive	Ol gray	Ol gray	Ol gray
Lithology:	Cc. ooze	Cc. ooze	Clay	Clay	Clay	Cc. ooze	Cc. ooze	Clay	Clay	Clay
Method:	XRF	XRF	XRF	DCP	XRF	XRF	XRF	XRF	XRF	DCP
SiO2	22.71	23.80	54.26	59.13	54.15	14.76	8.74	57.50	56.68	56.89
TiO2	.301	.295	.725	.742	.695	.209	.097	.781	.746	.738
Al2O3	6.69	5.78	15.02	16.16	14.51	4.34	1.61	15.92	15.38	15.78
FeO	2.54	2.08	5.63	5.11	4.86	1.46	.90	5.25	5.51	5.49
MnO	.198	.515	.330	.112	.131	.379	.265	.125	.163	.181
MgO	2.01	1.53	3.50	2.98	2.99	1.57	.73	3.15	3.52	3.37
CaO	30.97	32.39	2.21	.63	3.63	39.29	46.80	.97	.59	.57
Na2O	.67	.27	4.01	2.76	3.90	.26	.09	3.97	4.23	4.09
K2O	1.26	.98	2.65	2.76	2.47	.78	.37	2.48	2.53	2.81
P2O5	.164	.152	.166	.140	.155	.187	.064	.106	.127	.144
LOI	32.5	32.21	11.5	9.47	12.5	36.77	40.33	9.75	10.52	9.93
CaCO3	55.23	56.06	3.42		5.41	67.81	81.38	1.00	.58	
C (Org)	.63	.51	.82		.98	.74	.13	.67	.72	
Nb	4.7	4.9	10.3		9.8	3.4	1.3	10.9	10.5	
Zr	57.2	79.6	135.2	143.0	139.9	43.5	34.0	152.8	143.0	141.2
Y	17.2	20.9	26.2	28.5	27.1	16.7	6.8	25.1	25.2	26.3
Sr	1954	1171	204	143	244	1609	1117	154	152	153
Rb	51.3	41.3	113.7		104.2	32.4	12.9	109.6	107.9	
Zn	71.2	65.1	172.7	85.3	158.0	54.3	25.4	133.6	156.0	42.7
Cu	98.7	110.2	261.8	283.6	223.3	89.9	41.0	303.6	250.8	193.4
Ni	47	95	130	152	133	42	29	97	143	173
Cr	43.3	34.5	82.7	80.1	82.7	33.5	6.6	80.3	76.0	85.0
V	58	52	132	145	114	49	17	120	101	117
Ce	22.2	22.5	46.2		56.4	5.8	3.7	53.9	50.3	
Ba	671	1033	1383	1295	1328	791	301	1099	1262	1314
Sc				15.6						17.7

123-765B	3H-1, 33-35	4H-3, 145-150	4H-6, 20-22	4H-6, 23-30	5H-7, 40-42	7H-3, 38-43	8H-6, 85-90	9H-6, 104-105	10H-3, 145-150	10H-5, 89-95
Depth:	19.13	32.95	36.20	36.23	47.50	60.78	75.45	85.34	90.85	93.29
Color:	Lt olive		Red gray	Red gray	Lt olive	Lt ol gray	Lt ol gray	Gr gray		Lt gy blue
Lithology:	Cc. ooze		Clay	Clay	Cc. sand	Cc. ooze	Cc. ooze	Cc. ooze		Clay
Method:	XRF	DCP	XRF	DCP	XRF	XRF	XRF	XRF	DCP	DCP
SiO2	14.28	41.99	56.28	56.97	14.25	15.25	28.55	23.16	22.43	56.18
TiO2	.203	.538	.739	.704	.153	.227	.403	.351	.337	.889
Al2O3	4.40	11.16	14.78	14.88	2.95	4.56	8.70	7.32	6.04	18.86
FeO	1.56	3.57	5.45	6.35	1.24	1.63	3.22	2.67	2.22	6.47
MnO	.345	.100	1.217	.265	.080	.118	.122	.118	.184	.044
MgO	1.14	2.05	3.28	3.30	1.10	1.75	2.46	2.51	1.47	3.98
CaO	40.16	16.79	.83	.67	41.55	39.40	26.46	30.73	34.74	.36
Na2O	.02	1.67	3.75	3.61	.09	.44	1.40	1.08	.94	2.07
K2O	.75	1.87	2.42	2.70	.62	.85	1.31	1.23	1.13	3.29
P2O5	.134	.120	.105	.115	.066	.176	.142	.186	.143	.138
LOI	37.00	19.14	11.15	10.45	37.90	35.60	27.25	30.65	31.13	7.73
CaCO3	70.64		2.42		74.47	70.31	46.90	55.31		
C (Org)	.22		.91		.13	.58	.29	.66		
Nb	3.3		10.2		2.5	3.7	6.2	5.1		
Zr	38.5	150.9	150.4	145.3	44.7	46.9	80.9	62.1	99.7	198.5
Y	15.5	17.9	30.8	28.7	9.9	14.3	20.7	19.0	20.2	33.1
Sr	1381	531	171	163	1022	1967	998	1330	1142	160
Rb	28.7		100.6		22.0	31.4	61.9	53.2		
Zn	43.1	90.5	142.0	44.8	29.9	44.7	81.3	73.9	51.2	118.8
Cu	62.1	231.2	192.6	385.2	46.7	51.7	102.3	74.0	60.3	172.7
Ni	31	143	153	324	20	29	52	39	30	95
Cr	31.8	56.8	77.6	71.1	16.9	38.6	49.8	51.6	33.4	116.6
V	39	118	110	209	26	41	65	60	42	142
Ce	6.2		55.3		16.8	16.8	24.6	19.3		
Ba	902	750	1609	1282	341	482	1110	758	689	699
Sc		9.1		16.7					5.7	18.2

Table 1 (continued).

123-765B	11H-2, 40-44	12H-4, 44-48	12H-6, 105-110	13H-2, 138-143	14H-4, 83-87	15H-2, 76-88	15H-2, 88-100	15H-2, 115-127	15H-3, 1-13	15H-3, 20-32
Depth:	97.90	110.54	114.15	118.08	130.13	136.76	136.88	137.15	137.51	137.70
Color:	Lt ol gray	Lt ol gray	Ol gray	Lt ol gray	Lt ol gray	Lt ol gray	Ol gray	Lt ol gray	Lt gr yel	Lt ol gray
Lithology:	Cc. ooze	Cc. ooze	Clay	Cc. ooze	Cc. ooze	Cc. sand	Clay	Cc. ooze	Cc. ooze	Cc. sand
Method:	XRF	XRF	XRF	XRF	XRF	XRF	XRF	XRF	XRF	XRF
SiO2	23.07	16.17	56.42	20.29	20.93	22.80	54.56	18.50	21.20	14.82
TiO2	.338	.259	.967	.335	.349	.328	.971	.294	.319	.190
Al2O3	6.55	4.99	19.16	6.79	7.50	5.81	19.42	6.34	5.82	3.17
FeO	2.39	1.78	6.93	2.50	2.73	2.48	7.51	2.41	2.46	1.25
MnO	.103	.150	.048	.102	.095	.067	.039	.149	.130	.094
MgO	1.88	1.32	3.64	1.79	1.65	1.68	3.60	1.48	1.44	.92
CaO	33.40	39.98	.52	34.49	34.36	34.17	.41	36.00	34.84	41.79
Na2O	.64	.35	1.26	.77	.27	.75	1.89	.66	.68	.33
K2O	1.34	.85	3.07	1.23	1.37	1.17	3.18	1.31	1.25	.70
P2O5	.187	.158	.171	.201	.137	.156	.159	.109	.159	.111
LOI	30.1	34	7.8	31.5	30.6	30.59	8.26	32.73	31.7	36.64
CaCO3	61.89	69.81	.50	60.89	62.31	60.00	.50	63.47	59.64	73.22
C (Org)	.15	.04	.27	.31	.12	.30	.29	.05	.24	.08
Nb	4.7	4.1	13.8	5.1	5.6	4.4	13.5	4.5	4.6	2.9
Zr	80.0	62.2	208.9	74.7	70.4	88.0	199.2	66.1	88.9	68.6
Y	19.0	16.0	32.2	15.1	14.2	17.7	30.1	17.2	19.8	12.8
Sr	1229	1336	206	1506	1342	2024	214	1403	1192	1042
Rb	48.3	31.9	133.1	48.3	54.4	45.8	139.8	48.8	45.4	24.9
Zn	60.2	35.1	125.7	51.5	48.4	45.2	117.3	46.4	43.3	29.1
Cu	58.0	48.6	101.2	52.8	54.4	70.5	260.3	37.2	44.6	57.8
Ni	36	26	56	47	24	36	63	18	19	17
Cr	44.0	35.5	113.3	49.5	47.0	61.5	125.8	36.7	31.1	31.0
V	58	42	118	53	53	63	150	44	46	33
Ce	20.1	14.1	65.3	25.5	23.0	20.7	66.2	22.5	20.2	12.7
Ba	597	546	820	378	513	289	748	687	557	316
Sc										

123-765B	15H-3, 32-44	15H-5, 23-27	15H-5, 49-54	15H-5, 116-121	15H-7, 52-56	16H-1, 42-46	16H-1, 42-46	16H-1, 42-46	16H-1, 42-46	17H-5, 63-65
Depth:	137.82	140.73	140.99	141.66	144.02	144.62	144.62	144.62	144.62	160.53
Color:	Gy olive	Gr gray	Lt ol gray	Lt gr gray	Lt ol gray	Lt ol gray	Lt ol gray	Lt ol gray	Lt ol gray	Lt ol gray
Lithology:	Clay	Cc. clay	Cc. ooze	Cc. ooze	Cc. sand	Cc. sand	Cc. sand	Cc. sand	Cc. sand	Cc. sand
Method:	XRF	XRF	XRF	XRF	XRF	XRF	DCP	DCP	DCP	XRF
SiO2	53.89	35.56		21.69	24.42	25.16	24.44	24.20	24.45	39.75
TiO2	.971	.596		.359	.341	.334	.343	.330	.340	.200
Al2O3	19.07	11.82		7.91	7.05	6.66	6.77	6.73	6.76	2.73
FeO	7.45	4.72		2.80	2.53	2.43	2.49	2.43	2.50	1.62
MnO	.039	.051		.084	.074	.082	.083	.080	.084	.048
MgO	4.07	2.59		1.64	1.44	1.43	1.29	1.26	1.32	.48
CaO	.59	20.68		32.88	32.30	32.62	32.25	31.98	32.84	29.45
Na2O	1.78	.56		.65	.62	.46	1.09	1.10	1.10	.50
K2O	3.45	2.52		1.29	1.31	1.23	1.15	1.15	1.15	.95
P2O5	.139	.112		.113	.123	.106	.113	.100	.100	.071
LOI	8.56	20.80		30.60	29.80	29.50	30.26	29.50	30.26	24.20
CaCO3	1.17	36.49	58.81	58.48	57.48	57.23				51.98
C (Org)	.29	.31	.19	.11	.13	.13				.08
Nb	13.1	8.1	5.5	5.9	5.5	5.5				4.1
Zr	190.4	115.8	70.9	73.6	96.9	94.0	97.6	94.8	99.0	112.8
Y	28.3	19.6	15.8	14.8	16.0	15.2	15.6	15.9	15.6	7.9
Sr	222	1128	1325	1306	1143	1130	1107	1106	1106	782
Rb	147.8	99.2	57.7	55.9	49.2	46.7				26.4
Zn	140.7	71.5	53.9	51.5	47.0	45.6	49.0	45.3	47.4	19.8
Cu	324.9	33.6	42.6	64.5	64.4	61.4	49.4	47.3	48.9	50.1
Ni	86	35	22	26	25	21	25	20	25	29
Cr	127.3	73.9	51.7	45.6	42.7	41.5	43.6	38.6	48.9	9.2
V	134	85	56	56	51	50	56	46	60	27
Ce	69.8	43.4	25.5	33.0	26.7	28.5				15.5
Ba	810	351	633	591	490	462	435	432	430	251
Sc							6.3	7.1	7.2	

Table 1 (continued).

123-765B	18H-1, 13-19	18H-3, 145-150	19X-3, 20-26	20X-2, 125-129	21X-2, 145-150	21X-3, 64-70	22X-1, 94-97	23X-2, 91-97	24X-4, 77-83	26X-1, 69-73
Depth:	163.73	168.10	176.50	185.75	195.65	196.34	203.34	214.51	227.07	241.89
Color:	Gy olive	Lt ol gray	Lt brown	Yel gray		Gy green	Ol gray	Lt ol gray	Ol gray	Lt ol gray
Lithology:	Clay	Cc. ooze	Cc. sand	Cc. ooze		Clay	Cc. sand	Cc. ooze	Clay	Cc. sand
Method:	DCP	DCP	DCP	XRF	DCP	DCP	XRF	DCP	DCP	XRF
SiO2	52.18	15.68	15.77	14.43	8.01	52.69	18.13	14.26	47.16	6.68
TiO2	.922	.287	.132	.234	.130	.873	.179	.240	.697	.062
Al2O3	19.64	5.77	2.28	4.33	2.50	16.54	1.94	4.59	14.05	.69
FeO	6.59	2.00	1.56	1.69	1.31	5.47	1.65	1.50	4.30	.22
MnO	.035	.051	.053	.042	.064	.027	.029	.037	.024	.019
MgO	3.39	1.11	.68	1.68	1.69	5.75	1.94	2.79	7.68	1.12
CaO	2.27	39.39	43.28	40.97	45.65	2.66	41.10	39.71	6.93	49.87
Na2O	1.77	.71	1.07	.13	.53	1.98	.17	.91	1.56	.08
K2O	2.97	.83	.56	.67	.40	2.54	.41	.70	2.19	.19
P2O5	.198	.122	.105	.123	.110	.287	.143	.091	.137	.064
LOI	10.04	34.4	35.17	35.7	39.27	11.18	34.3	36.74	15.27	41
CaCO3				74.72			73.80			91.96
C (Org)				.00			.07			.00
Nb				3.3			2.3			1.0
Zr	196.7	66.5	80.1	55.2	27.9	184.5	93.2	49.5	150.1	38.7
Y	34.3	12.2	9.1	7.7	8.2	33.8	6.1	9.0	21.6	2.1
Sr	327	1564	1179	2086	1861	399	2565	2194	541	1624
Rb				25.4			13.3			5.4
Zn	103.7	38.2	38.6	31.6	25.5	77.3	13.5	25.9	51.3	4.9
Cu	170.1	25.1	55.9	160.0	12.8	109.0	36.5	13.9	74.2	25.7
Ni	135	19	36	25	10	63	23	13	35	1
Cr	145.5	38.6	20.3	41.0	24.9	120.9	21.7	47.9	114.7	.0
V	133	38	21	39	27	121	16	33	115	3
Ce				20.0			10.2			1.5
Ba	579	277	178	151	185	511	93	143	202	75
Sc	21.1	4.8	2.1		2.4	19.0		5.4	18.6	

Table 1 (continued).

123-765B	36X-2, 81-86	37X-CC, 19-25	39X-1, 20-26	39X-1, 86-91
Depth:	340.21	350.70	366.90	367.56
Color:	Lt olive	Lt gr gray	Gy olive	
Lithology:	Chalk	Chalk	Dol. clay	
Method:	DCP	DCP	DCP	DCP
SiO2	5.51	11.57	41.60	3.07
TiO2	.108	.214	.539	.041
Al2O3	2.01	3.89	10.57	.41
FeO	.63	1.31	3.35	.16
MnO	.026	.017	.033	.022
MgO	2.07	2.94	9.15	2.20
CaO	48.87	41.71	12.25	50.77
Na2O	.62	.68	1.28	.33
K2O	.30	.47	1.16	.08
P2O5	.062	.054	.178	.022
LOI	41.25	37.87	19.89	43
CaCO3				
C (Org)				
Nb				
Zr	26.3	43.3	141.2	36.1
Y	6.6	7.8	29.2	4.0
Sr	3233	3671	903	2593
Rb				.0
Zn	15.9	24.9	59.7	6.9
Cu	13.1	21.1	38.9	7.2
Ni	3	10	54	2
Cr	24.1	49.2	93.7	12.9
V	14	34	97	12
Ce				.0
Ba	133	145	236	26
Sc	2.8	5.3	13.2	

123-765B	26X-3, 72-77	27X-1, 41-46	28X-1, 34-38	29X-2, 21-25	30X-1, 86-92	31X-3, 140-150	32X-2, 126-129	33X-2, 71-73	34X-CC, 17-23	35X-2, 37-42
Depth:	244.92	251.31	260.94	271.91	280.76	294.00	302.06	311.21	321.90	330.17
Color:	Lt olive	Gr gray	Lt olive	Ol gray	Lt gr gray		Lt gr gray	Lt gr gray	Ol gray	Br gray
Lithology:	Cc. ooze	Cc. ooze	Cc. ooze	Cc. sand	Chalk		Cc. sand	Chalk	Cc. sand	Cc. siltst.
Method:	XRF	XRF	XRF	DCP	DCP	DCP	XRF	XRF	DCP	DCP
SiO2	18.65	13.75	10.20	12.78	12.99	10.71	8.91	17.24	44.92	12.56
TiO2	.303	.225	.153	.105	.175	.192	.154	.286	.147	.181
Al2O3	5.60	4.27	2.93	1.50	3.84	3.66	2.92	5.98	2.06	3.20
FeO	1.64	1.26	.96	.45	1.35	1.08	1.05	1.81	.51	1.22
MnO	.021	.021	.033	.028	.027	.036	.012	.028	.014	.020
MgO	2.97	2.96	2.39	1.39	3.87	2.73	2.92	2.73	.84	2.31
CaO	36.22	40.24	44.39	45.07	38.73	43.21	41.47	36.53	26.96	42.11
Na2O	.32	.33	.19	.50	.80	.52	.25	.25	.40	.77
K2O	.99	.73	.46	.31	.51	.54	.49	1.08	.76	.52
P2O5	.079	.106	.095	.059	.092	.073	.075	.070	.054	.079
LOI	33.20	36.10	38.20	37.85	36.92	38.26	41.74	34.00	23.87	37.61
CaCO3	68.89	74.89	80.88				82.22	68.81		
C (Org)	.13	.26	.25				.13	.01		
Nb	4.1	2.8	1.8				2.3	4.0		
Zr	46.3	47.0	34.5	90.2	41.1	40.5	38.1	60.3	96.5	63.7
Y	8.3	6.3	5.2	6.6	8.5	7.4	5.5	8.3	6.5	9.7
Sr	2729	2846	3252	1625	2657	2759	3186	2405	1049	2600
Rb	40.5	30.3	16.9				18.8	42.5		
Zn	29.2	36.8	19.6	23.6	25.3	25.9	18.5	32.6	19.4	23.5
Cu	39.3	38.4	49.5	7.7	12.2	39.7	40.7	34.3	9.8	77.6
Ni	12	10	7	2	11	13	11	13	3	20
Cr	52.9	41.9	24.9	11.8	36.9	33.6	24.8	47.4	13.2	34.4
V	45	30	20	10	34	34	23	46	16	27
Ce	23.6	14.9	3.2				9.6	15.8		
Ba	129	110	124	92	120	136	141	163	174	168
Sc				1.4	5.0	2.7			1.4	4.5

123-765C	2R-2, 90-99	3R-1, 131-133	4R-3, 140-150	5R-3, 45-49	6R-1, 143-149	7R-2, 27-32	8R-2, 114-120	10R-3, 140-150	11R-1, 84-88	11R-1, 91-93
Depth:	362.00	370.61	383.40	392.05	399.73	409.77	420.34	440.90	446.84	446.91
Color:	Lt ol gray	Br black		Lt gr gray	Ol gray	Gy green	Olive		Ol gray	Lt ol gray
Lithology:	Chalk	Dol. clay		Cc. silt	Chalk	Clay	Cc. ooze		Cc. clay	Chalk
Method:	DCP	DCP	DCP	DCP	DCP	DCP	DCP	DCP	XRF	DCP
SiO2	7.38	49.77	13.50	17.67	11.46	51.09	30.45	27.04	36.94	9.63
TiO2	.100	.730	.152	.256	.162	.810	.466	.283	.620	.162
Al2O3	1.89	13.75	3.15	4.95	2.69	17.07	9.88	6.61	12.50	3.13
FeO	.61	3.64	.79	1.52	.83	4.82	3.18	2.12	4.11	1.11
MnO	.061	.030	.040	.052	.037	.044	.038	.056	.050	.086
MgO	2.88	9.56	3.50	3.85	2.19	6.59	4.25	5.47	4.33	1.73
CaO	44.49	4.43	39.93	36.41	43.55	3.62	22.54	27.11	18.21	45.88
Na2O	.57	1.09	.52	.57	.79	1.40	1.11	.70	1.03	.41
K2O	.21	1.39	.28	.52	.37	2.02	.85	.53	1.45	.35
P2O5	.050	.181	.052	.059	.056	.108	.039	.043	.157	.041
LOI	41.77	15.44	37.58	33.93	38.00	12.44	27.20	28.84	20.60	38.22
CaCO3									32.90	
C (Org)									.31	
Nb									9.2	
Zr	33.6	166.1	31.9	69.2	50.9	179.2	100.2	60.3	122.1	39.5
Y	7.8	27.3	6.9	10.0	8.8	27.6	13.1	9.0	21.4	7.8
Sr	2794	422	2498	1683	3630	447	2486	1950	702	1098
Rb									64.4	
Zn	16.8	74.6	26.3	39.7	22.1	104.4	67.7	47.5	94.8	25.2
Cu	32.0	55.9	9.6	24.0	25.0	221.0	13.6	17.2	119.9	10.1
Ni	13	44	9	19	15	74	28	21	60	15
Cr	28.8	129.6	38.7	49.3	43.6	139.1	87.4	59.0	98.1	30.6
V	31	139	36	46	38	152	87	57	92	29
Ce									49.4	
Ba	113	114	116	171	90	199	81	66	160	89
Sc	5.2	16.9	2.3	5.0	3.5	18.0	10.1	5.0		3.5

Table 1 (continued).

123-765C	11R-1, 93-96	11R-1, 96-97	11R-1, 97-100	11R-1, 119-123	11R-1, 133-137	11R-4, 61-64	11R-4, 61-64	13R-2, 61-64	14R-1, 97-104	15R-1, 86-104
Depth:	446.93	446.96	446.97	447.19	447.33	451.11	451.11	466.71	475.07	484.56
Color:	Lt ol gray	Lt ol gray	Lt ol gray	Lt ol gray	Lt ol gray	Gy blue	Gy blue	Gy olive	Yel brown	Bl gr gray
Lithology:	Chalk	Chalk	Cc. ooze	Cc. ooze	Cc. sand	Clay	Clay	Clay	Clay	0
Method:	DCP	DCP	XRF	XRF	XRF	XRF	DCP	XRF	DCP	DCP
SiO_2	9.23	8.97	9.83	11.17	11.44	55.39	55.19	54.53	52.18	60.99
TiO_2	.158	.156	.158	.159	.112	.977	.998	.905	.919	.964
Al_2O_3	2.99	2.86	3.00	2.54	1.32	18.52	18.83	18.54	20.83	18.26
FeO	1.09	1.02	1.13	.99	.73	5.77	5.84	8.54	8.74	5.58
MnO	.096	.101	.093	.106	.097	.067	.061	.049	.103	.034
MgO	1.68	1.66	1.73	1.84	1.46	5.82	5.72	2.96	3.83	2.30
CaO	46.38	47.22	45.40	44.72	46.97	.41	.40	1.54	.42	.59
Na_2O	.38	.36	.17	.20	.12	1.29	1.35	1.72	1.70	1.45
K_2O	.34	.32	.40	.37	.31	1.94	1.95	2.14	2.13	2.19
P_2O_5	.042	.040	.051	.081	.051	.200	.222	.097	.148	.243
LOI	38.37	38.5	38.04	37.82	37.4	9.62	9.43	8.99	9	7.4
$CaCO_3$			81.80	80.72	83.80	1.08		4.08		
C (Org)			.00	.09	.04	.18		.00		
Nb			2.4	2.7	1.6	15.1		10.5		
Zr	36.9	36.8	37.3	49.7	43.2	199.5	181.8	156.7	174.4	188.1
Y	6.8	6.5	6.1	7.5	4.1	37.6	34.6	18.3	30.0	45.0
Sr	1069	1066	1068	1585	1426	386	362	452	334	313
Rb			13.2	12.3	8.5	93.4		92.0		
Zn	25.7	23.2	20.1	19.4	10.4	160.4	148.4	126.7	151.6	141.1
Cu	9.7	9.6	23.0	39.9	26.5	313.6	320.2	70.6	146.1	116.0
Ni	13	13	13	14	9	101	109	56	113	45
Cr	29.0	29.5	28.8	20.4	13.0	135.3	118.0	104.1	135.6	120.3
V	26	28	26	30	20	148	152	139	106	181
Ce			10.0	11.0	9.4	83.9		52.7		
Ba	97	105	114	105	116	164	154	226	132	442
Sc	3.4	3.3					18.0		16.9	16.4

123-765C	17R-2, 66-68	19R-1, 21-27	20R-1, 77-84	22R-2, 28-32	23R-4, 62-69	24R-1, 92-93	24R-1, 92-93	24R-4, 71-72	25R-1, 92-97	25R-2, 92-98
Depth:	504.56	521.50	531.57	551.88	564.82	570.22	570.22	574.51	579.92	581.42
Color:	Lt brown	Lt gr gray	Yel brown	Gy olive	Gy orange	Gy brown	Gy brown	Br gray	Lt brown	Br gray
Lithology:	Cc. ooze	Silty ooze	Clay	Clay	Chalk	Clay	Clay	Clay	Cc. ooze	Clay
Method:	XRF	DCP	DCP	XRF	DCP	XRF	DCP	XRF	DCP	XRF
SiO_2	25.48	24.64	62.30	62.24	16.45	57.27	57.16	55.54	10.26	55.72
TiO_2	.454	.231	.439	.601	.217	1.018	1.016	.940	.166	1.055
Al_2O_3	9.39	5.87	11.92	14.49	5.48	15.70	15.56	15.23	3.52	16.10
FeO	3.61	2.62	8.33	5.43	2.36	9.17	9.18	7.38	1.45	8.99
MnO	.248	.361	.119	.059	.133	.089	.095	1.698	.169	.525
MgO	1.04	1.40	3.69	3.87	.88	3.72	3.82	4.46	.70	3.82
CaO	30.37	32.88	.93	1.82	38.98	.67	.66	.97	45.68	.85
Na_2O	.72	.93	2.73	2.28	.51	1.42	1.58	1.82	.29	1.65
K_2O	.94	.94	2.61	2.12	.81	3.78	3.90	3.54	.30	3.70
P_2O_5	.084	.104	.283	.141	.071	.285	.287	.339	.085	.295
LOI	27.68	30.03	6.66	6.94	34.11	6.87	6.74	8.07	37.40	7.30
$CaCO_3$	54.23			2.42		.33		.67		.42
C (Org)	.00			.04		.03		.00		.03
Nb	5.7			10.0		15.9		13.6		12.2
Zr	84.5	60.7	86.5	127.5	47.5	197.3	198.4	160.4		168.7
Y	12.9	23.0	36.3	26.6	19.5	48.5	50.5	71.0		60.3
Sr	1125	729	666	374	763	130	136	204		161
Rb	37.9			70.5		116.3		104.6		113.2
Zn	62.9	38.6	124.6	84.9	42.9	140.3	133.1	149.5		162.7
Cu	35.0	69.5	266.6	82.2	25.0	67.9	72.8	165.5		178.7
Ni	39	26	57	128	25	81	92	118		109
Cr	56.6	38.0	52.6	97.5	30.5	68.9	75.9	66.1		87.5
V	84	57	83	152	59	113	133	137		131
Ce	31.8			52.3		101.2		150.7		107.7
Ba	221	387	74	409	1219	213	222	2941	3282	822
Sc		6.6	10.2		5.9		23.9			

Table 1 (continued).

123-765C	25R-3, 106-111	25R-3, 106-111	26R-4, 22-28	26R-4, 42-51	27R-2, 34-40	28R-1, 55-58	28R-3, 45-53	29R-3, 76-80	29R-5, 2-6	29R-5, 26-30
Depth:	583.06	583.06	593.02	593.22	599.34	607.55	610.45	620.16	622.42	622.66
Color:	Br gray	Br gray	Brown	Br gray	Br gray	Br gray	Gy green	Gy blue/gr	Lt brown	Lt brown
Lithology:	Clay	Clay	Clay	Clay	Clayst.	Clayst.	Cc. Clayst	Clayst.	Clay	Clay
Method:	XRF	DCP	XRF	DCP	XRF	XRF	XRF	XRF	DCP	DCP
SiO_2	56.24	56.58	55.50	56.80	57.16	58.06	45.78	56.62	57.94	58.01
TiO_2	.962	.958	1.002	1.058	1.036	.976	.712	.841	1.114	.964
Al_2O_3	16.70	16.76	15.06	16.92	16.60	17.18	12.19	16.22	15.95	16.72
FeO	7.66	7.70	7.35	7.72	7.34	7.56	5.80	5.88	8.69	8.10
MnO	1.138	1.181	.106	1.077	1.898	.866	.108	.106	.119	.131
MgO	3.24	3.36	3.71	3.59	3.17	2.84	2.53	2.70	3.49	3.28
CaO	.98	.98	3.43	.59	.52	.47	13.20	3.54	.59	.64
Na_2O	1.76	1.70	1.63	1.68	1.72	1.77	1.69	2.15	1.98	2.09
K_2O	3.52	3.74	3.51	3.66	4.06	4.10	3.00	3.93	4.11	4.14
P_2O_5	.357	.353	.276	.111	.131	.099	.109	.106	.117	.115
LOI	7.46	6.69	8.43	6.8	6.36	6.08	14.88	7.9	5.9	5.8
$CaCO_3$	.50		4.83		.25	.17	22.24	5.33		
C (Org)	.03		.02		.01	.01	.11	.06		
Nb	15.4		14.1		14.4	13.4	10.1	11.8		
Zr	175.3	175.7	176.6	170.3	169.1	157.0	115.7	142.3	172.6	163.4
Y	71.7	70.4	59.1	26.8	25.1	19.3	23.7	21.3	28.7	28.8
Sr	176	181	147	145	229	169	289	172	129	148
Rb	108.8		100.4		109.7	115.8	86.8	120.0		
Zn	165.4	165.1	127.2	128.6	135.7	165.0	116.1	149.5	123.5	128.4
Cu	183.1	202.1	105.2	143.1	151.5	142.3	49.6	257.2	82.4	130.9
Ni	136	138	79	99	102	95	70	81	92	85
Cr	78.7	83.5	81.4	72.9	60.9	74.8	55.7	71.1	96.9	82.7
V	134	147	93	121	127	136	87	132	108	104
Ce	153.8		98.2		132.4	122.3	69.6	89.3		
Ba	2235	2090	204	1651	2610	871	1834	539	221	218
Sc		23.2		22.5					21.8	22.1

123-765C	29R-5, 70-74	29R-5, 124-129	30R-2, 16-22	30R-2, 16-22	30R-3, 76-83	30R-4, 98-102	32R-1, 40-45	33R-2, 117-124	34R-3, 115-125	35R-3, 24-29
Depth:	623.10	623.64	627.56	627.56	629.66	631.38	645.40	657.37	668.55	677.34
Color:	Lt brown	Lt brown	Gy brown	Gy brown	Brown	Brown	Yel brown	Gr gray	Lt brown	Gy blue/gr
Lithology:	Clay	Cc. clay	Clayst.	Clayst.	Clayst.	Clayst.	Clayst.	Clay	Cc. clay	Clayst.
Method:	DCP	DCP	XRF	DCP	DCP	XRF	DCP	DCP	DCP	XRF
SiO_2	58.99	55.04	59.79	57.82	59.21	59.08	63.32	62.66	61.99	68.61
TiO_2	.884	.791	.968	.937	.873	.878	.849	.706	.276	.740
Al_2O_3	17.34	16.81	17.51	17.13	17.63	16.98	14.04	14.12	5.17	12.71
FeO	7.20	6.57	7.09	6.85	6.55	7.29	6.14	7.31	2.07	4.83
MnO	.127	.166	1.542	1.536	.199	.148	.104	.100	.501	.040
MgO	2.77	2.60	2.95	2.89	2.58	2.62	2.90	2.73	1.05	2.86
CaO	.64	3.89	.79	.78	.70	.71	.68	.83	12.41	.68
Na_2O	2.12	2.11	2.24	2.03	2.40	2.32	2.54	2.57	1.09	1.85
K_2O	4.25	3.91	3.84	3.84	3.86	3.66	3.61	2.56	.95	2.13
P_2O_5	.102	.120	.123	.122	.099	.098	.097	.105	.085	.132
LOI	5.60	8.00	3.15	6.07	5.90	6.21	5.71	6.30	13.97	5.41
$CaCO_3$			.67			.17				.33
C (Org)			.03			.05				.13
Nb			13.2			10.6				14.0
Zr	146.4	144.2	145.3	145.2	134.2	131.6	131.3	97.0	44.6	134.4
Y	24.7	31.4	27.1	30.6	21.3	19.3	26.4	19.9	13.4	25.1
Sr	166	207	207	210	212	227	262	201	185	123
Rb			112.1			110.9				76.4
Zn	135.2	112.9	141.8	140.8	121.1	135.4	112.4	94.2	34.4	125.0
Cu	129.0	122.1	142.4	157.1	113.1	97.0	146.8	37.5	68.2	327.5
Ni	81	77	79	79	67	74	77	39	15	91
Cr	75.5	73.1	65.3	69.4	72.6	64.3	67.4	70.5	37.0	55.1
V	118	109	120	130	114	108	91	137	53	113
Ce			126.0			92.7				115.8
Ba	233	1364	1135	1143	233	232	199	811	2098	940
Sc	20.5	21.6		21.9	19.3		16.9	14.9	6.0	

Table 1 (continued).

123-765C	35R-3, 86-90	37R-3, 40-43	39R-3, 101-105	39R-3, 140-150	40R-3, 104-109	42R-2, 41-43	44R-2, 38-42	44R-2, 73-77	44R-2, 95-99	44R-2, 119-123
Depth:	677.96	696.40	715.71	716.10	724.94	741.71	760.38	760.73	760.95	761.19
Color:	Black	Ol gray	Ol gray		Br black	Gy green	Ol gray	Ol gray	Ol gray	Ol gray
Lithology:	Siltst.	Cc. Clayst	Clayst.		Clayst.	Clayst.	Clayst.	Clayst.	Clayst.	Clayst.
Method:	XRF	XRF	XRF	DCP	XRF	XRF	DCP	DCP	DCP	DCP
SiO2	80.64	43.10	65.71	52.63	66.79	75.27	64.74	67.24	65.31	67.25
TiO2	.282	.480	.831	.552	.799	.551	.835	.764	.672	.730
Al2O3	4.88	7.57	12.44	9.14	11.58	9.41	13.22	12.80	12.69	12.94
FeO	1.72	4.57	7.22	5.06	7.90	4.90	7.49	6.70	6.52	6.53
MnO	.019	.577	.180	.279	.050	.141	.293	.060	1.505	.066
MgO	.89	1.92	2.95	2.17	3.05	1.92	2.69	2.51	2.33	2.44
CaO	2.91	19.66	1.07	11.44	.70	.58	.69	.46	.67	.49
Na2O	1.16	1.18	1.75	1.40	1.58	1.24	1.58	1.53	1.53	1.55
K2O	.74	1.45	2.49	1.82	2.19	1.66	2.68	2.54	2.24	2.51
P2O5	.064	.140	.165	.160	.110	.100	.197	.101	.128	.100
LOI	6.7	19.35	5.19	13.51	5.24	4.23	5.6	5.3	6.4	5.4
CaCO3	4.66	34.65	1.00		.50	.58				
C (Org)	.67	.04	.04		.22	.15				
Nb	3.2	7.0	11.3		12.5	7.4				
Zr	.0	85.9	126.7	95.9	138.4	100.4	138.3	123.0	117.9	120.9
Y	11.2	30.1	28.8	25.9	21.7	20.2	31.2	20.7	24.6	19.7
Sr	88	249	138	198	98	117	100	88	99	94
Rb	31.3	47.2	76.8		69.4	61.4				
Zn	42.8	99.4	126.1	105.8	102.6	77.3	186.4	83.1	84.3	89.0
Cu	35.0	104.2	119.0	121.9	242.1	81.1	210.8	183.1	126.2	176.8
Ni	18	70	73	70	71	30	97	38	63	37
Cr	40.3	34.2	45.2	50.1	44.9	38.3	61.7	59.0	55.3	59.3
V	42	65	120	79	220	87	145	140	130	136
Ce	12.4	63.6	111.0		72.8	60.8				
Ba	389	3560	613	2223	153	1927	418	486	818	741
Sc				12.4			17.0	15.4	15.0	15.6

123-765C	44R-4, 55-59	45R-2, 70-75	47R-5, 46-55	50R-1, 110-113	51R-1, 84-86	52R-2, 110-118	53R-1, 66-72	54R-3, 140-150	55R-4, 2-8	57R-1, 111-117
Depth:	763.55	770.40	793.86	816.70	825.84	837.10	844.76	857.90	867.52	882.81
Color:	Ol gray	Dusky red	Gy brown	Brown	Dk gray	Gy olive	Brown	Pink gray	Br gray	Brown
Lithology:	Clayst.	Clayst.	Clayst.	Clayst.	Clayst.	Clayst.	Rad clayst	Rad ooze	Rad clayst	Clayst.
Method:	XRF	XRF	DCP	XRF	XRF	DCP	DCP	DCP	DCP	DCP
SiO2	69.14	71.91	69.02	70.15	74.89	71.44	73.39	81.08	59.86	72.49
TiO2	.700	.670	.973	.759	.774	.524	.554	.315	.393	.515
Al2O3	12.09	10.95	11.84	9.34	9.05	8.77	8.58	5.18	7.19	9.03
FeO	6.55	5.83	6.09	8.42	5.02	5.67	6.59	3.21	2.42	6.00
MnO	.140	.040	.051	.080	.060	1.389	.203	.052	1.536	.644
MgO	2.25	2.19	2.69	2.63	2.35	2.38	2.45	1.36	2.07	2.50
CaO	.64	.65	.75	.62	.56	1.02	.75	.49	11.70	1.04
Na2O	1.42	1.35	1.37	1.31	1.24	1.14	1.16	.94	.99	1.23
K2O	2.18	1.91	2.21	1.95	1.96	2.20	1.97	1.16	1.07	1.63
P2O5	.089	.154	.108	.099	.100	.270	.156	.115	.174	.212
LOI	4.80	4.34	4.90	4.64	4.00	5.20	4.20	3.74	12.60	4.70
CaCO3	1.08	.67		.58	.42					
C (Org)	.29	.09		.01	.18					
Nb	10.8	9.9		11.3	10.4					
Zr	136.2	122.5	122.1	126.7	97.2	81.7	101.9	61.7	130.7	134.6
Y	17.6	27.2	22.6	25.1	21.4	28.9	26.5	18.2	42.2	37.7
Sr	98	122	95	91	76	127	113	238	274	190
Rb	71.2	65.1		54.4	54.1					
Zn	110.8	55.6	98.5	90.8	74.1	57.6	80.5	66.8	99.9	88.6
Cu	179.8	200.6	613.2	87.7	111.9	79.6	127.9	109.4	805.9	85.3
Ni	50	43	50	43	34	101	53	63	88	52
Cr	49.8	56.2	46.3	33.5	29.5	36.8	31.9	25.2	26.3	26.1
V	129	120	149	65	99	84	49	40	130	45
Ce	67.8	63.7		78.8	67.2					
Ba	492	1797	510	1257	467	2860	2688	9669	5185	5961
Sc			14.4			12.3	15.6	11.3	9.6	11.4

Table 1 (continued).

123-765C	58R-4, 67-71	59R-4, 39-45	60R-5, 120-123	60R-5, 120-123	61R-4, 92-94	61R-5, 81-85	61R-5, 81-85	62R-3, 73-79	62R-3, 80-84	62R-4, 19-21
Depth:	896.37	902.79	914.70	917.00	922.32	923.71	923.71	930.13	930.20	931.09
Color:	Brown	Gy red	Brown	Brown	Brown	Gy brown	Gy brown	Gy brown	Gy brown	Gy brown
Lithology:	Clayst.	Clayst.	Ash	Ash	Ash	Cc.Clayst	Cc.Clayst	Clayst.	Clayst.	Clayst.
Method:	XRF	DCP	DCP	XRF	XRF	XRF	DCP	DCP	XRF	DCP
SiO2	74.20	69.68	62.84		56.30	45.56	44.92	65.81	65.65	60.25
TiO2	.543	.537	.235		.865	.687	.680	.814	.829	.814
Al2O3	8.69	12.08	19.15		13.58	8.35	8.39	10.90	10.46	10.48
FeO	5.87	5.54	1.11		4.24	6.95	6.88	7.98	8.00	14.46
MnO	.212	.043	.108		.113	1.627	1.557	2.257	2.325	.092
MgO	2.48	2.85	5.89		4.03	2.23	1.90	2.60	2.70	2.92
CaO	.68	.92	1.45		6.28	15.35	15.52	.76	.86	1.20
Na2O	1.22	1.39	2.37		1.65	.81	.92	1.22	1.17	1.19
K2O	1.55	1.83	.56		2.12	2.28	2.40	3.06	3.11	3.37
P2O5	.156	.131	.075		.145	.118	.115	.172	.242	.437
LOI	4.41	5	6.22		10.67	16.05	18.33	4.43	4.66	4.80
CaCO3	.33				9.58	27.32			.50	
C (Org)	.01				.02	.00			.00	
Nb	11.0			10.7	90.6	9.7			13.8	
Zr	111.3	84.8	168.0	182.7	432.6	127.6	138.7	142.2	179.7	143.0
Y	31.9	21.4	8.6	7.8	48.3	30.6	31.4	30.4	44.0	55.4
Sr	143	135	136	150	138	130	129	139	139	82
Rb	48.8			6.7	46.8	54.7			83.3	
Zn	114.2	71.8	158.4	191.7	230.7	102.2	92.1	160.9	137.1	123.6
Cu	56.3	115.6	32.7	30.1	21.7	141.4	129.5	176.1	168.4	33.8
Ni	58	39	225	215	100	74	67	145	114	150
Cr	22.7	31.9	18.6	13.3	14.7	16.7	24.7	39.6	24.2	38.0
V	31	70	528	590	2297	95	74	129	138	490
Ce	96.3			17.0	178.4	81.4			86.7	
Ba	3870	2845	350	241	293	207	223	1883	1492	135
Sc		12.8	7.3				14.3	16.3		16.4

Oxides in wt%; elements in ppm. Abbrev: light (lt), dark (dk), olive (ol), gray (gy), green (gr), brown (br), black (bl), yellow (yell), calcareous (cc), claystone (clayst), siltstone (siltst), dolomitic (dol), radiolarian (rad).

Table 2. Instrumental neutron activation analyses (INAA) of Site 765 sediments.

123-765B	3H-1-35	4H-6-23	9H-6-98	10H-5-89	16H-1-42	16H-1-42	16H-1-42	16H-1-42	16H-1-50	17H-5-56	18H-1-13
Depth:	19.15	36.23	85.28	93.29	144.62	144.62	144.62	144.62	144.70	160.46	163.73
Color:	Lt olive	Red gray	Gr gray	Lt gy blue	Lt ol gray	Lt ol gray	Lt ol gray	Lt ol gray	Lt ol gray	Lt ol gray	Gy olive
Lithology:	Cc. ooze	Clay	Cc. ooze	Clay	Cc. sand	Cc. sand	Cc. sand	Cc. sand	Cc. sand	Cc. sand	Clay
Powder:	AI	AI	AI	AI	WC	WC	WC	WC	AI	AI	AI
La	13.7	30.0	19.5	36.7	17.6	17.6	17.6	17.6	17.5	8.3	41.6
Ce	19.7	63.2	30.8	67.2	30 7	30.7	30.7	30.7	30.8	15.1	73.7
Nd	11.4	26.9	16.0	27.9	13.2	13.2	13.2	13.2	13.4	6.6	31.5
Sm	2.34	5.57	3.22	6.29	2.78	2.78	2.78	2.78	2.93	1.30	6.78
Eu	.522	1.259	.707	1.303	.582	.582	.582	.582	.550	.280	1.376
Tb	.393	.882	.468	.835	.461	.461	.461	.461	.404	.206	.902
Yb	1.42	2.79	1.90	3.23	1.59	1.59	1.59	1.59	1.58	.78	3.10
Lu	.239	.426	.282	.466	.245	.245	.245	.245	.255	.141	.566
Cs	1.93	6.15	3.65	7.84	3.00	3.00	3.00	3.00	3.10	1.23	7.79
Ba	842	1212	719	681	427	427	427	427	468	197	553
Sc	5.10	16.78	8.74	20.21	7.41	7.41	7.41	7.41	7.58	3.08	20.29
Hf	1.45	4.49	2.21	5.01	2.94	2.94	2.94	2.94	2.71	1.87	5.98
Ta	.297	.767	.442	.931	.883	.883	.883	.883	.483	.210	1.160
W	1.21	3.19	2.21	3.73	65.57	65.57	65.57	65.57	6.98	.61	9.38
Cr	31.7	73.7	53.8	105.8	42.1	42.1	42.1	42.1	41.2	21.9	119.4
Co	6.36	48.68	9.13	23.62	10.76	10.76	10.76	10.76	6.72	5.98	14.96
As	2.19	16.94	2.92	3.48	2.69	2.69	2.69	2.69	3.45	4.12	5.09
Sb	.566	10.387	.817	.769	.437	.437	.437	.437	.426	.797	.682
Th	3.77	10.81	6.05	13.57	6.47	6.47	6.47	6.47	6.39	3.14	16.87
U	1.52	1.61	3.14	1.83	1.37	1.37	1.37	1.37	1.53	1.72	2.16

123-765B	22X-1-88	26X-1-63	28X-1-28	39X-1-20
Depth:	203.28	241.83	260.88	366.90
Color:	Ol gray	Lt ol gray	Lt olive	Gy olive
Lithology:	Cc. sand	Cc. sand	Cc. ooze	Dol. clay
Powder:	AI	AI	AI	AI
La	5.9	3.3	7.0	20.9
Ce	12.9	6.1	12.7	41.0
Nd	6.3	2.0	5.3	19.6
Sm	1.16	.50	1.11	4.22
Eu	.258	.117	.265	.793
Tb	.207	.090	.176	.590
Yb	.75	.29	.56	1.90
Lu	.114	.048	.095	.263
Cs	.68	.44	1.44	4.04
Ba	140	92	16	264
Sc	2.10	.83	3.15	11.10
Hf	2.78	1.00	1.13	3.54
Ta	.218	.097	.207	.615
W	1.00	.61	.86	2.22
Cr	20.2	8.7	34.9	93.1
Co	2.74	.55	2.16	9.13
As	3.54	.46	1.05	3.65
Sb	.436	.063	.201	.600
Th	2.45	1.33	2.60	7.75
U	2.22	1.00	1.76	1.44

Table 2 (continued).

123-765C	2R-2-90	7R-2-27	11R-1-84	11R-1-88	11R-1-133	11R-4-61	11R-4-61	14R-1-97	17R-2-60	22R-2-28	23R-4-62
Depth:	362.00	409.77	446.84	446.88	447.33	451.11	451.11	475.07	504.50	551.88	564.82
Color:	Lt ol gray	Gy green	Ol gray	Lt ol gray	Lt ol gray	Gy blue	Gy blue	Yel brown	Lt brown	Gy olive	Gy orange
Lithology:	Chalk	Clay	Cc. clay	Chalk	Cc. sand	Clay	Clay	Clay	Cc. ooze	Clay	Chalk
Powder:	AI	AI	WC	AI	WC	WC	WC	AI	AI	WC	AI
La	4.9	31.1	26.2	11.4	5.4	39.4	39.4	32.1	16.7	22.4	17.2
Ce	7.1	64.6	50.2	21.9	8.6	81.1	81.1	72.7	30.5	50.0	30.4
Nd	4.1	26.3	21.5	7.7	4.0	31.9	31.9	22.5	11.0	18.8	12.3
Sm	.78	5.57	4.51	1.75	.84	6.94	6.94	5.20	2.50	4.38	2.70
Eu	.196	.989	.916	.377	.201	1.450	1.450	1.008	.515	.877	.519
Tb	.142	.702	.686	.262	.150	.996	.996	.654	.367	.620	.380
Yb	.48	2.51	2.23	1.10	.52	3.47	3.47	2.92	1.53	2.50	1.40
Lu	.058	.409	.319	.185	.063	.567	.567	.509	.260	.335	.197
Cs	.70	7.10	5.55	1.78	.58	7.99	7.99	8.70	3.79	4.91	1.96
Ba	117	243	204	112	126	164	164	171	206	477	1138
Sc	2.14	15.40	12.32	4.19	1.60	18.33	18.33	18.29	8.48	12.94	4.86
Hf	.70	4.96	3.82	1.35	1.24	5.69	5.69	5.24	2.48	3.63	1.32
Ta	.148	.855	.787	.257	.997	1.193	1.193	.916	.498	.917	.324
W	.13	2.63	10.86	2.69	145.84	13.32	13.32	4.33	2.17	24.85	1.35
Cr	27.3	140.0	96.2	34.8	16.7	119.6	119.6	138.8	58.1	92.5	26.6
Co	2.41	21.69	15.68	7.16	19.64	43.75	43.75	23.37	11.41	163.78	8.68
As	.73	4.46	2.84	3.53	1.87	4.20	4.20	12.43	9.11	1.52	5.24
Sb	.126	1.177	1.253	.350	.194	1.548	1.548	1.024	.551	.448	.317
Th	1.31	11.22	8.15	2.80	1.62	11.02	11.02	9.53	5.16	11.90	5.12
U	1.10	1.92	1.92	1.54	1.61	1.74	1.74	1.49	.70	1.12	.36

Table 2 (continued).

123-765C	25R-1-92	25R-3-106	25R-3-106	26R-4-22	26R-4-42	27R-2-34	28R-3-45	30R-4-98	35R-3-24	35R-3-86	37R-3-40
Depth:	579.92	583.06	583.06	593.02	593.22	599.34	610.45	631.38	677.34	677.96	696.40
Color:	Lt brown	Br gray	Br gray	Brown	Br gray	Br gray	Gy green	Brown	Gy blue/gr	Black	Ol gray
Lithology:	Cc. ooze	Clay	Clay	Clay	Clay	Clayst.	CcClayst	Clayst.	Clayst.	Siltst.	CcClayst
Powder:	Al	WC	WC	WC	Al	WC	WC	WC	WC	WC	WC
La	22.2	65.4	65.4	50.1	29.2	30.6	30.2	31.7	44.3	11.3	30.0
Ce	19.1	157.5	157.5	101.1	156.0	131.2	77.3	96.5	122.7	19.6	76.2
Nd	17.5	59.1	59.1	48.7	23.1	24.1	24.8	25.5	34.3	9.7	27.8
Sm	3.82	13.64	13.64	11.24	5.56	6.04	5.80	5.59	8.42	1.88	6.18
Eu	.883	2.844	2.844	2.320	1.087	1.152	1.155	1.172	1.375	.520	1.289
Tb	.514	1.766	1.766	1.618	.652	.730	.698	.677	.939	.328	.826
Yb	2.19	5.10	5.10	4.69	2.65	2.80	2.51	2.20	2.46	1.17	2.64
Lu	.330	.810	.810	.733	.342	.392	.387	.365	.324	.195	.434
Cs	1.39	6.32	6.32	5.57	5.43	6.33	5.08	7.46	4.73	2.06	2.92
Ba	3138	2149	2149	222	1505	2375	1865	243	1032	363	3578
Sc	5.39	22.75	22.75	23.24	23.70	22.76	16.80	20.39	19.30	6.18	13.32
Hf	.95	5.35	5.35	5.29	4.73	5.19	3.54	4.33	4.04	1.19	2.66
Ta	.173	1.231	1.231	.934	.861	1.080	.783	.969	.995	.290	.636
W	.63	13.29	13.29	12.21	5.14	8.92	4.83	16.62	5.50	7.62	12.56
Cr	17.5	81.0	81.0	84.5	69.3	66.6	63.9	70.4	64.1	37.1	39.5
Co	7.75	78.51	78.51	17.07	37.25	51.62	20.22	26.33	35.58	9.94	28.82
As	.97	6.37	6.37	4.52	5.59	5.87	1.26	8.21	39.67	16.53	1.55
Sb	.123	.725	.725	.521	.678	.624	.690	.417	1.020	.405	.425
Th	1.70	12.32	12.32	11.22	9.78	9.93	8.69	11.55	13.08	3.66	6.46
U	.25	1.07	1.07	.79	.96	.97	.79	.92	2.17	1.48	.50

Table 2 (continued).

123-765C	39R-3-101	44R-4-55	45R-2-70	50R-1-110	58R-4-67	61R-5-81	62R-3-73	62R-3-80	62R-3-80
Depth:	715.71	763.55	770.40	816.70	896.37	923.71	930.13	930.20	930.20
Color:	Ol gray	Ol gray	Dusky red	Brown	Brown	Gy brown	Gy brown	Gy brown	Gy brown
Lithology:	Clayst.	Clayst.	Clayst.	Clayst.	Clayst.	CcClayst	Clayst.	Clayst.	Clayst.
Powder:	WC	WC	WC	WC	WC	WC	Al	WC	WC
La	36.9	27.4	31.4	35.3	38.3	41.9	43.0	54.2	54.2
Ce	117.8	69.9	77.7	88.7	113.6	78.3	84.5	94.2	94.2
Nd	32.6	23.3	29.0	31.7	31.2	34.7	37.0	47.2	47.2
Sm	8.14	5.07	6.57	7.06	6.65	8.11	8.56	10.81	10.81
Eu	1.452	1.058	1.304	1.452	1.460	1.771	1.734	2.248	2.248
Tb	.938	.620	.866	.920	.893	1.083	1.156	1.482	1.482
Yb	2.67	1.92	2.69	2.72	2.79	3.29	3.55	4.40	4.40
Lu	.379	.317	.437	.430	.460	.476	.504	.634	.634
Cs	4.26	4.04	3.79	2.92	2.56	3.08	5.24	5.12	5.12
Ba	691	507	1921	1287	4155	227	2175	1473	1473
Sc	18.31	15.09	15.21	15.46	15.10	17.39	16.37	16.67	16.67
Hf	3.86	3.91	3.54	3.75	3.26	4.39	4.85	5.42	5.42
Ta	.995	.918	.866	.931	.856	.891	.911	1.179	1.179
W	13.62	28.09	19.51	17.09	29.05	49.12	4.74	40.43	40.43
Cr	51.7	54.0	55.3	44.5	33.3	27.3	33.5	34.5	34.5
Co	36.44	31.38	15.58	22.53	32.46	25.73	27.97	29.71	29.71
As	2.90	15.39	5.03	8.36	15.42	16.87	13.39	13.88	13.88
Sb	.679	.567	.927	.770	1.060	.649	.817	.945	.945
Th	9.78	8.53	9.28	6.81	7.56	7.62	9.89	10.22	10.22
U	.80	.91	1.34	.65	.53	.55	.99	1.13	1.13

All elements in ppm. See Table 1 for major and trace element analyses for samples or adjacent intervals.
Powdering method: tungsten carbide shatterbox (WC), alumina ball mill (Al). Other abbreviations as in Table 1.

Table 3. Precision and accuracy of DCP and XRF analyses.

	IOBC DCP n = 10	% st dev	SCO-1 XRF	SCO-1 Accepted Values	SCO-1 New
SiO_2	52.33	.27	68.22	68.74	68.22
TiO_2	.864	1.67	.750	.688	.685
Al_2O_3	18.71	.77	15.18	14.97	15.18
FeO	11.61	.72	5.72	5.63	5.61
MnO	2.08	1.42	.060	.058	.062
MgO	3.38	1.04	2.98	3.01	2.89
CaO	2.03	1.86	2.80	2.87	2.71
Na_2O	4.09	1.39	.950	.990	1.049
K_2O	2.93	2.22	3.00	3.03	3.00
P_2O_5	1.17	2.86	.210	.226	.239
LOI	9.65	3.34			
Total	99.19				
Nb			13.0	11.2	11.3
Zr	187	4.64	176	163	166
Y	174	4.44	24.0	26.6	22.8
Sr	204	1.24	164	178	177
Rb			115	114	115
Zn	74	4.61	107	105	107
Cu	266	8.04	27.0	29.3	30.5
Ni	368	1.20	34.0	27.6	28.1
Cr	89	2.23	64.0	69.5	74.2
V	207	2.72	144	134	134
Ce			57.0	63.3	51.2
Ba	358	1.48	543	582	613
Sc	24	2.12			

Oxides in wt%; elements in ppm.

data that are routinely reported (smear slides, XRD analyses, visual core descriptions, etc.). If geochemical variability can be tied to lithologic variability, then potentially accurate estimates of sediment sections might be made, based only on published core descriptions and a few chemical analyses. Thus, an important first step is to examine the relationship between the geochemical and the lithological variations in Site 765 sediments.

Dilution

The first-order control for variability of almost all the elements analyzed in Site 765 sediments is dilution by calcium carbonate (cc) (Ludden, Gradstein, et al., 1990). An element such as Al, for instance, is quantitatively diluted by cc. Figure 2 shows that as cc varies from 0 to 100 wt%, Al_2O_3 varies from about 20 to 0 wt%. Cc is present in Site 765 sediments largely as nannoplankton and foraminifer skeletons that were transported to the site via turbidity flows. A typical calcareous turbidite consists of a foraminiferal sand at the base (almost 100% cc), and a long interval of featureless olive nannofossil ooze that grades upward to a white nannofossil ooze that is often bioturbated (see Dumoulin et al., this volume). Intervals between turbidites typically consist of green clay, with essentially no cc. Because the cc content may vary from 0% to almost 100% in a single turbidite sequence (including the clay-rich interval), the entire compositional range of the hole for an element such as Al can be observed on the centimeter to meter scale of a single graded sequence. Calcareous lithologies are much less common in the Cretaceous section, and so a first-order depth variation in most elements is lower concentrations in the Cenozoic section from dilution by calcareous turbidites and an increase with depth from the predominance of clay-rich lithologies.

A few elements (Sr, U, Ba, and P) do not show cc dilution relationships because they take part in the biologic cycles of the oceans. For example, U and Sr are taken into the carbonate shells of marine organisms. Ba and P are often enriched below zones of high biological productivity (Schmitz, 1987; Toyoda et al., 1990, and references therein). Mn exhibits a complex distribution that is not related to cc dilution, but may reflect post-burial mobility from its redox chemistry (Compton, this volume).

Although a large part of the variation in most element concentrations results from cc dilution, significant variation at low cc contents also exists. Examination of just the low cc samples shows another dilution effect caused by silica (Fig. 2). Thus, almost all of the Al_2O_3 variation in Site 765 sediments may be explained by dilution of an end-member with about 20% Al_2O_3, by cc and silica. The excess silica reflects either radiolarian-rich intervals or detrital quartz. Figures 3A and 3C show good agreement between SiO_2/Al_2O_3 (which is insensitive to cc dilution) and radiolarian abundances in the sediments. The scattered high Si_2O/Al_2O_3 values in the upper 500 m of the section mark coarse-grained bases of turbidites, where detrital quartz and heavy minerals may concentrate (Zr and Ti also may be enriched in these

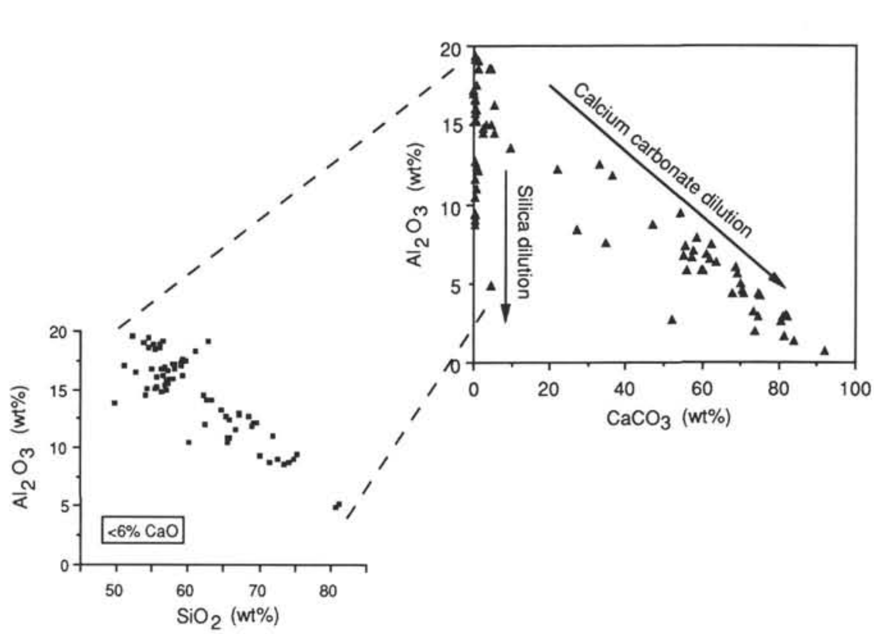

Figure 2. Al_2O_3 vs. $CaCO_3$, and Al_2O_3 vs. SiO_2 for a subset of low carbonate samples (<6 wt% CaO) that exhibit dilution effects on Site 765 sediments.

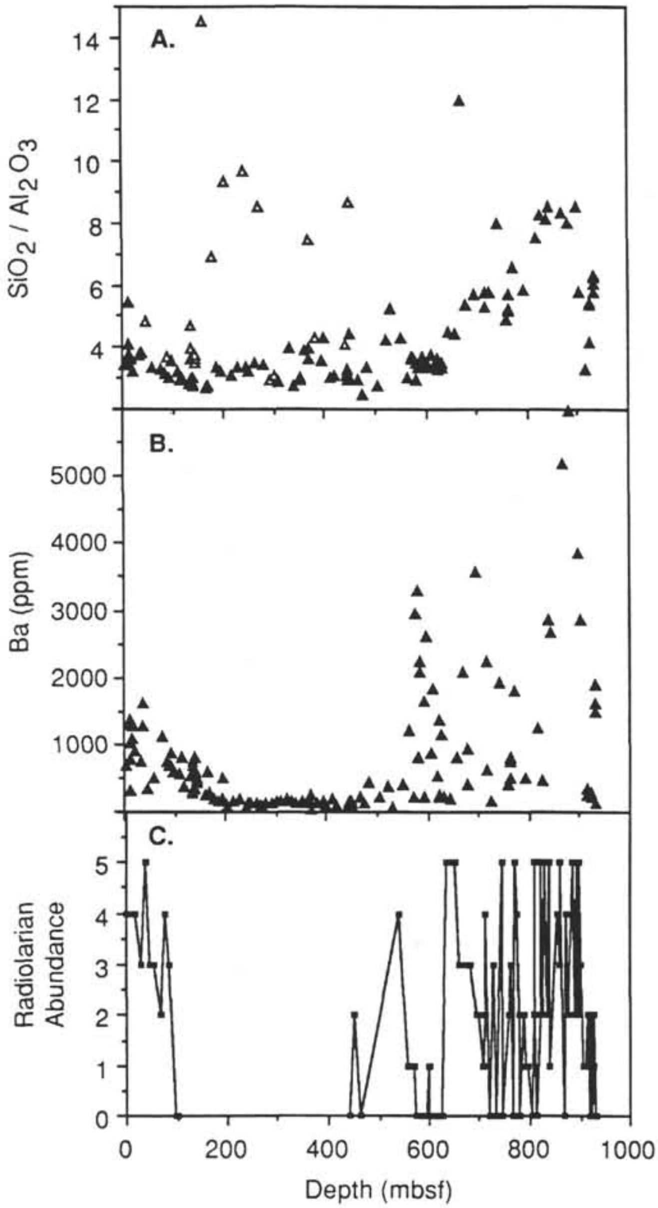

Figure 3. Dependence of SiO_2 and Ba on radiolarian abundances at Site 765. **A.** SiO_2/Al_2O_3 (wt% ratio) of sediments vs. depth. Open triangles represent turbidite bases enriched in detrital quartz. **B.** Ba contents of sediments vs. depth. **C.** Radiolarian abundances in sediments vs. depth (from Table 9 in Ludden, Gradstein, et al., 1990). All three variables are high in the upper 100 m and lower 600 m of Site 765.

intervals). Sediments having high abundances of siliceous fossils often have high Ba contents (Schmitz, 1987, and references therein). The highest Ba contents in Site 765 sediments (up to 10,000 ppm) occur in the radiolarian-rich interval between 800 and 900 mbsf, and a rough correspondence exists between Ba and radiolarian distributions (Figs. 3B and 3C).

Although the largest control on concentrations of elements in Site 765 sediments is cc and silica dilution, some elements vary significantly even after removing the effects of dilution. Most of the dilution signal can be removed by normalizing element concentrations to Al, because Al is quantitatively diluted by cc and silica. In addition, Al is associated almost exclusively with the detrital phase in sediments; thus elements that form constant ratios with Al are diagnostic of the composition of the detrital phase. In a later section, we will discuss the provenance of the detrital phase in Site 765 sediments. First, however, we will discuss those elements that do not form constant ratios with Al, but instead reflect changes in sediment mineralogy or lithology down the hole.

Mg, Cr, and Sr in Diagenetic Clays and Carbonates

Figures 4 and 5 show anomalously high MgO/Al_2O_3, Cr/Al_2O_3 and Sr values in the interval between 200–400 mbsf. This interval contains an unusual mineral association: aragonite, dolomite, and the magnesian clay minerals, palygorskite and sepiolite (Compton and Locker, this volume). Because of the intimate intergrowths of

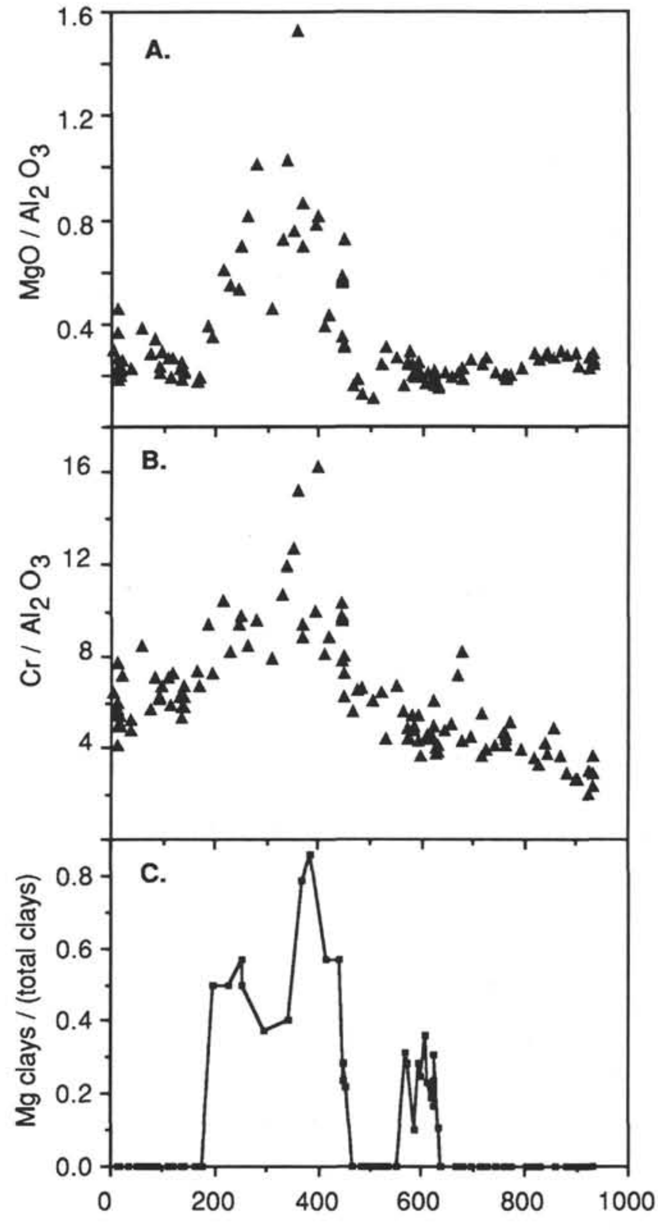

Figure 4. Enrichment of Mg and Cr in magnesian clay minerals at 200 to 400 mbsf at Site 765. **A.** MgO/Al_2O_3 (wt% ratio) in sediments. **B.** Cr (ppm)/Al_2O_3 (wt%) in sediments. **C.** Proportion of magnesian clays (palygorskite, sepiolite, and I/S/C) relative to total clays, as estimated by Compton and Locker (this volume).

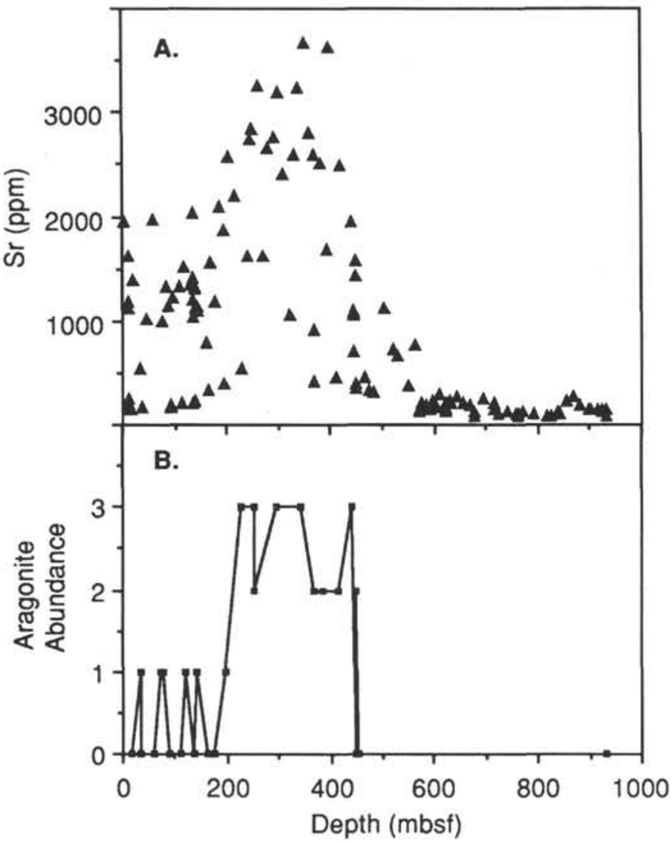

Figure 5. **A.** Sr contents of Site 765 sediments. **B.** Aragonite abundances from Compton and Locker (this volume). Sr is enriched in aragonite relative to clays and calcite.

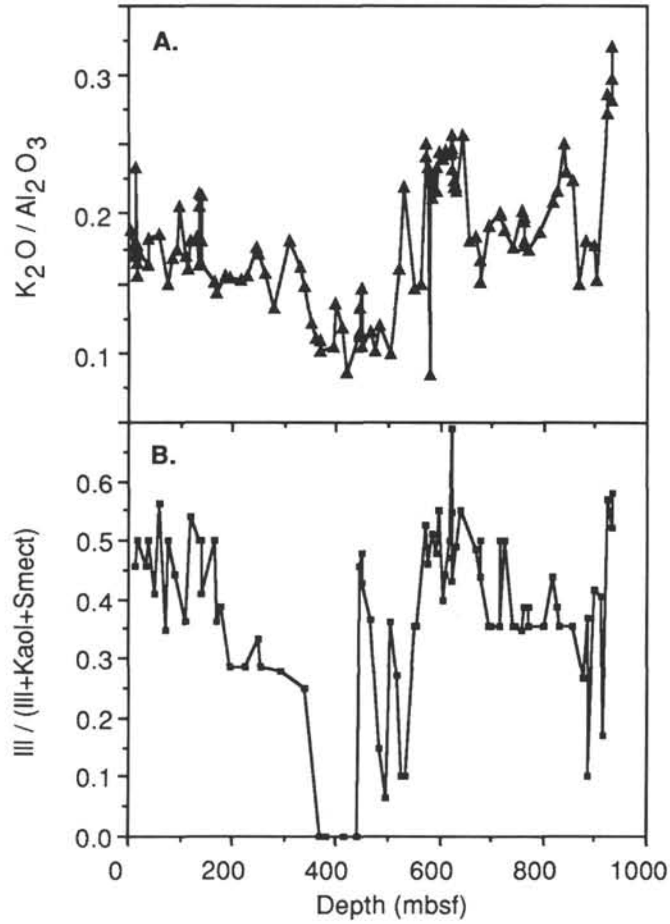

Figure 6. Dependence of K_2O content of Site 765 sediments on clay mineralogy. **A.** K_2O/Al_2O_3 (wt% ratio) of sediments. **B.** Proportion of illite relative to sum of illite, kaolinite, and smectite (I/S <10%) from Compton and Locker (this volume).

dolomite and fragile palygorskite fibers, Compton and Locker (this volume) favor a diagenetic origin for the magnesian clay minerals. The bulk composition of the sediments reflects this mineral association: Sr is high because aragonite is enriched in Sr over calcite (Figs. 5A, 5B); MgO is high because of the presence of dolomite and the magnesian clays (Figs. 4A, 4C). Compton and Locker (this volume) suggest that diffusion from seawater supplies the Mg required to form the diagenetic dolomite and clay minerals. The high Cr/Al_2O_3 values (Fig. 4B) are less easily explained; either the source of the sediments in this interval was enriched in Cr, or the diagenetic reactions that led to the formation of the magnesian clays favored Cr enrichment. We are unaware of any published accounts of Cr-rich varieties of palygorskite or sepiolite.

Potassium and Clay Minerals

K_2O/Al_2O_3 varies by more than a factor of two in Site 765 sediments (Fig. 6A), and variations in this ratio appear to reflect variations in the clay mineralogy (after Compton and Locker, this volume). The K_2O content of the bulk sediments varies roughly with the percentage of illite (a high K clay mineral) relative to the K-barren clay minerals, kaolinite and smectite (Figs. 6A, 6B). The low K_2O/Al_2O_3 values around 400 m reflect dominance of kaolinite, while the peak around 600 m reflects high illite and K-feldspar contents.

Iron, Manganese, and Cretaceous Clays

Both FeO/Al_2O_3 and Mn/Al_2O_3 increase dramatically at about 600 mbsf (Figs. 7A, 7B), which corresponds roughly with the Cretaceous/Tertiary boundary. The Cretaceous section at Site 765 is characterized by a decrease in abundance of cc turbidites, a decrease in sedimentation rate, an increase in amount of pelagic clay, and an increase in (volcanogenic) smectite (Ludden, Gradstein, et al., 1990). Several of these factors may have led to an increase in the Fe and Mn contents of these sediments. The smectite that dominates the lower 600 m is Fe-rich and Al-poor relative to the detrital illite and kaolinite that dominate the upper 600 m (Compton and Locker, this volume). Thus, the increase in abundance of smectite in the lower section is partly responsible for the increase in FeO/Al_2O_3. The slower sedimentation rates in the Cretaceous section, in part reflecting a decrease in rapidly deposited turbidite sequences, favors enrichment and preservation of the Fe-Mn oxyhydroxides that constantly rain onto the seafloor. Thus, Cretaceous sediments have a higher hydrogenous component and higher Fe and Mn contents. Finally, FeO and MnO are anomalously high in the clays immediately overlying the basaltic basement (Figs. 7A, 7B), suggesting a ridge hydrothermal origin for some of the Fe and Mn.

REE Abundances, Patterns, and Ce Anomalies

Like Fe and Mn, the rare earth elements (REE) increase dramatically in the lower 600 m (Fig. 8A). A higher hydrogenous component in Cretaceous sediments might have led to higher REE contents because Fe-Mn oxyhydroxide flocs scavenge REEs from the water column (Aplin, 1984, and references therein) and may enrich underlying sediments. However, Sm correlates well with

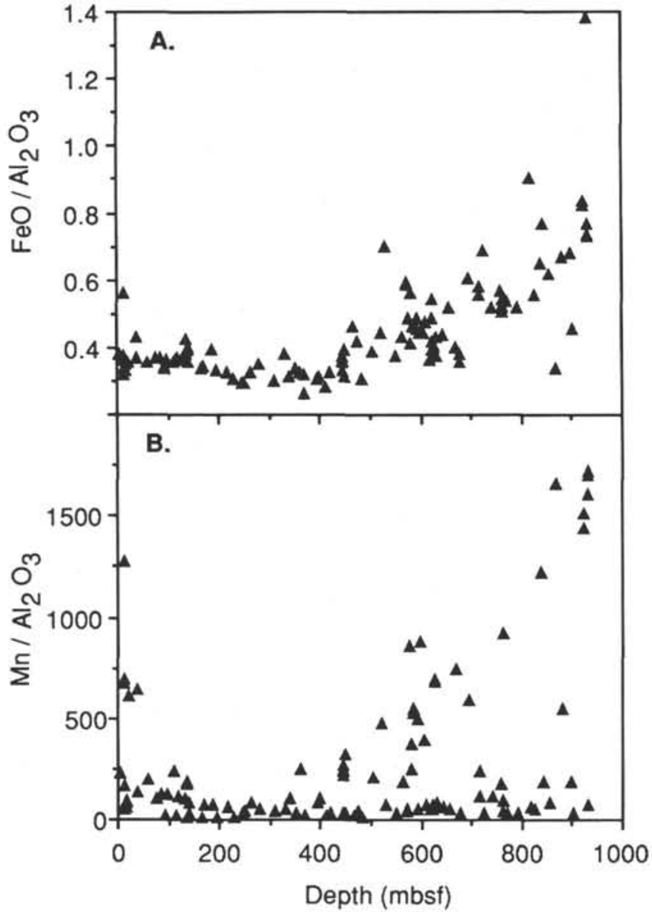

Figure 7. Increasing FeO and Mn in the lower 600 m of Site 765. **A.** FeO/Al_2O_3 (wt% ratio) in sediments. **B.** Mn (ppm)/Al_2O_3 (wt%) in sediments.

P_2O_5 in Site 765 clays, and the correlation is similar to that of recent Pacific pelagic clays (Fig. 9). One might thus speculate that phosphate phases, such as fish teeth and bones, exert a dominant control on abundances of the REEs in Site 765 sediments, similar to what has been suggested for recent Pacific pelagic sediments (Toyoda et al., 1990). Low sedimentation rates and high biological activity may have led to higher biogenic phosphate contents in pelagic clays (Toyoda et al., 1990).

The chondrite- or shale-normalized REE patterns also exhibit differences between Cenozoic and Cretaceous samples (Figs. 10A and 10B). The REE patterns of the Cretaceous sediments are typically enriched in the middle REEs, producing concave downward shale-normalized REE patterns (Fig. 10B) and high Sm/Yb contents (Fig. 8B). The hydrogenous and phosphate phases, as well as the volcanic source of the smectites in the Cretaceous sediments, may all contribute different REE patterns, and Sm/Yb does not correlate simply with any of these components.

Ce anomalies form in the marine environment as a result of the contrasting behavior of oxidized Ce^{4+} relative to the other dominantly trivalent REEs. Fe-Mn flocs preferentially scavenge Ce^{4+} from seawater, which leads to positive Ce anomalies in Mn nodules and hydrogenous Fe-Mn crusts and a negative anomaly in seawater (Elderfield and Greaves, 1981, and references therein). Site 765 sediments exhibit both positive and negative Ce anomalies, with positive anomalies more common in Cretaceous sediments (Fig. 8C). The magnitude of the Ce anomaly is consistent within three different sediment types (Fig. 11). First, samples having the largest positive Ce anomalies are high in Mn, reflecting

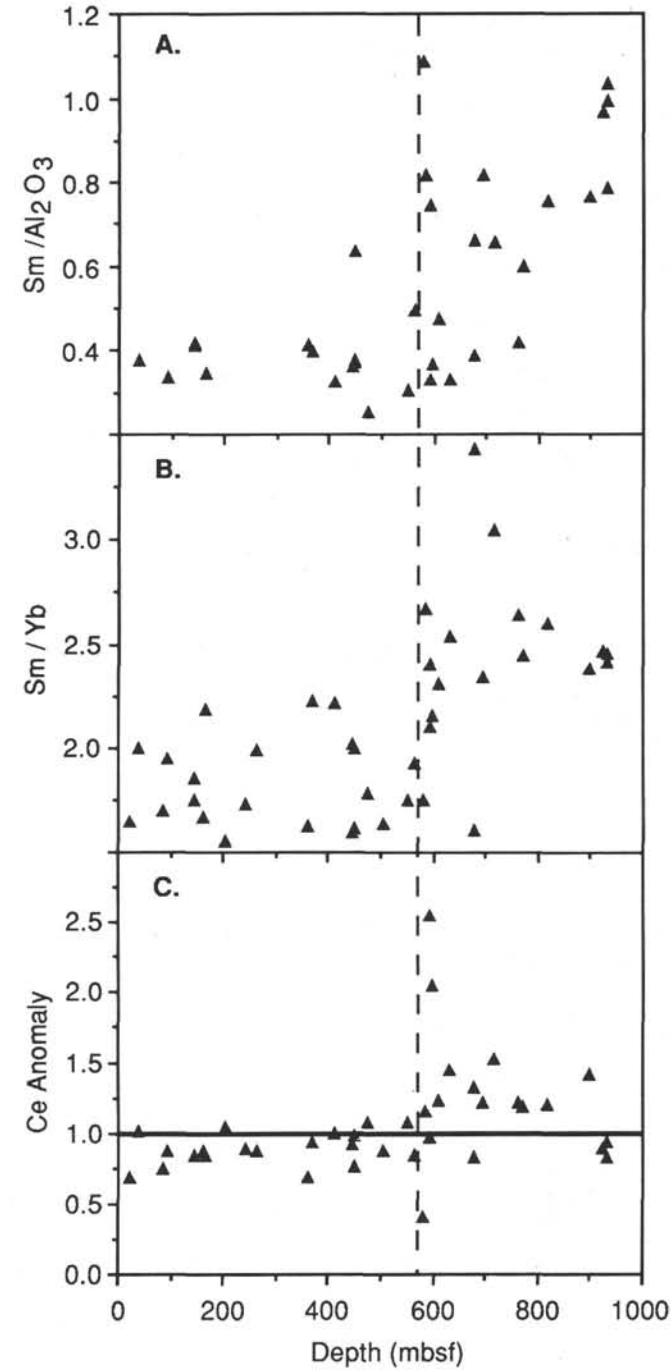

Figure 8. Variations in the REEs with depth at Site 765. Dashed line indicates approximate position of the Cretaceous/Tertiary boundary. **A.** Sm (ppm)/Al_2O_3 (wt%) is higher in Cretaceous sediments. **B.** Sm/Yb (ppm ratio) shows greater heavy REE-depletion in Cretaceous sediments. **C.** Ce anomaly reflects Ce deviation from La and Nd in chondrite-normalized patterns and may be calculated from $[3Ce_n/(2La\,n = n + Nd_n)]$, where n indicates chondrite-normalized concentrations. Ce anomalies are generally negative (<1.0) in Cenozoic samples and are more commonly positive (>1.0) in Cretaceous sediments.

a significant hydrogenous component that has scavenged REEs from seawater. Second, cc-rich sediments have negative Ce anomalies. Foraminifer tests, although almost devoid of REEs themselves, may become coated by an authigenic Fe-Mn oxide phase rich in REEs (Palmer, 1985). These oxide phases have been

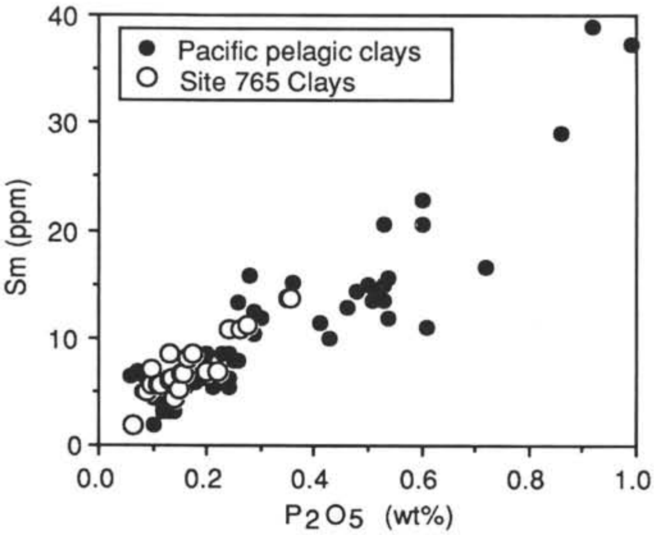

Figure 9. Sm and P_2O_5 in recent Pacific pelagic clays (from Toyoda et al., 1990) and Site 765 clays (<6.0 wt% CaO).

shown to possess negative Ce anomalies inherited from bottom water (Palmer, 1985). Finally, clay-rich samples have Ce anomalies that depend upon their P_2O_5 contents, showing a relationship identical to recent Pacific pelagic sediments (Toyoda et al., 1990). Phosphate phases (such as fish teeth) may have large negative Ce anomalies (Elderfield and Pagett, 1986, and references therein), and so increasing amounts of phosphate may lead to larger negative Ce anomalies.

This analysis of the REEs in Site 765 sediments suggests that downhole variations in abundances of REEs and their patterns are dependent upon downhole variations in phosphate, Mn, and cc phases. In general, phases enriched in REEs (clay, phosphate, and Mn) dominate the Cretaceous, while REE-poor cc dominates the Cenozoic sediments (see Fig. 75 in Ludden, Gradstein, et al., 1990). In detail, however, distribution of the Mn and phosphate phases may be complex (Figs. 7B, 12). Nonetheless, high P_2O_5 contents are typical of the 450- to 600-m interval (Fig. 12). This interval is distinguished by the lowest sedimentation rates in the hole (1–2 m/m.y.), where fish debris may not be overwhelmed by other influxes. Even so, the P_2O_5 contents in this interval require less than 1% apatite (with about 40% P_2O_5), which may explain why fish debris was not identified in sediment smear slides. Because fish-bone apatite may contain on the order of 100 times the REE contents of shales (Elderfield and Pagett, 1986; Staudigel et al., 1985/86; Toyoda et al., 1990), this seemingly trivial amount becomes significant.

Although minor phases and lithologies may be important for affecting downhole variations in certain elements, the aim of this study is to characterize the *average* composition of Site 765 sediments. In this regard, the most volumetrically significant control on element concentrations in Site 765 sediments is dilution of a shalelike phase with cc. For example, although subtle differences in REE patterns may reflect different mineral phases, all Site 765 sediments, and in fact all marine sediments, have REE patterns remarkably similar to average shale. This justifies the practice of normalizing REE to average shales. Although K_2O/Al_2O_3 varies with clay mineralogy (Figs. 6A, 6B), the average value is similar to average shale (around 0.2 for Australian shales; Taylor and McLennan, 1985). In the following section, we

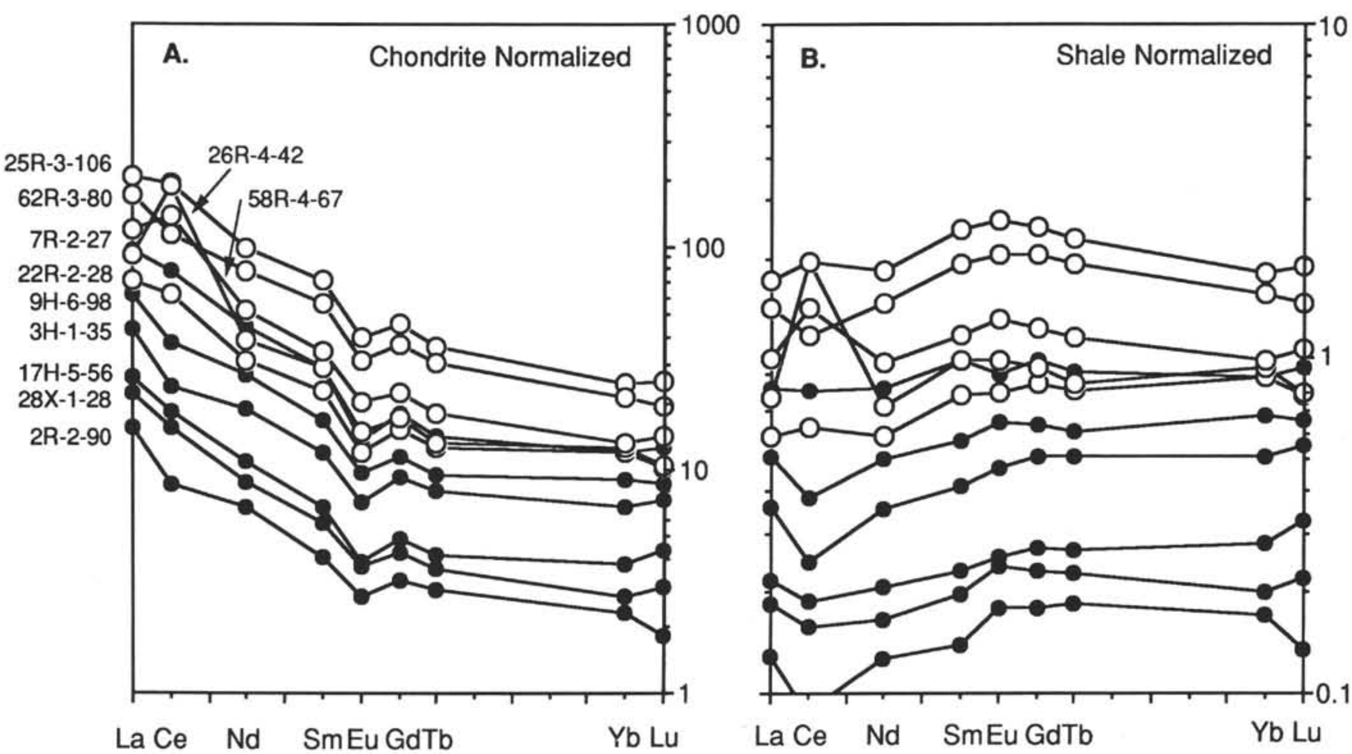

Figure 10. REE patterns in selected Site 765 sediments. Gd has been interpolated between Tb and Sm to illustrate Eu anomalies better. Closed circles indicate Cenozoic sediments; open circles represent Cretaceous sediments. **A.** Chondrite-normalized patterns (to values in Taylor and Gorton, 1977). **B.** Shale-normalized patterns (to PAAS in Taylor and McLennan, 1985).

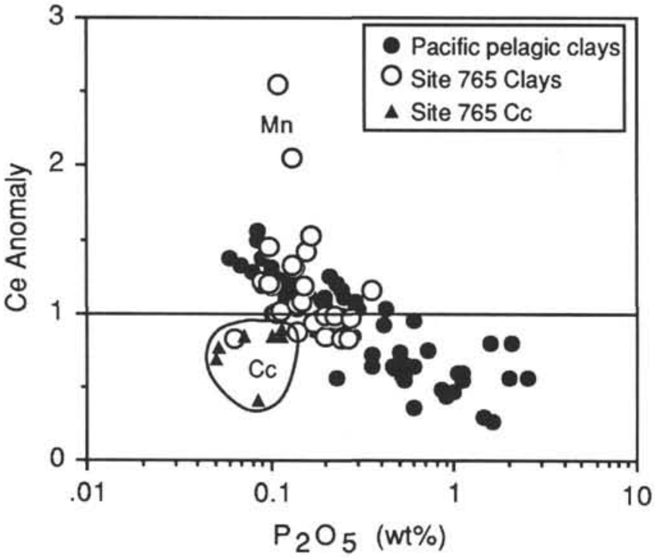

Figure 11. Ce anomalies in Site 765 clays, carbonates (>20% CaO), and Mn-rich clays. Carbonates have negative Ce anomalies; Mn-rich clays have positive anomalies. Other Site 765 clays exhibit a similar relationship between Ce anomaly and P_2O_5 content as recent Pacific pelagic clays (Toyoda et al., 1990).

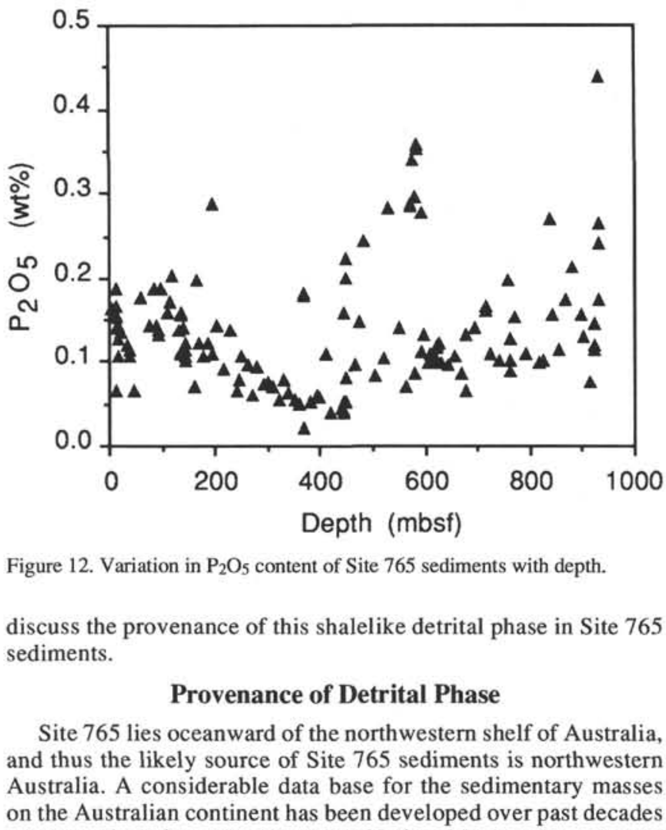

Figure 12. Variation in P_2O_5 content of Site 765 sediments with depth.

discuss the provenance of this shalelike detrital phase in Site 765 sediments.

Provenance of Detrital Phase

Site 765 lies oceanward of the northwestern shelf of Australia, and thus the likely source of Site 765 sediments is northwestern Australia. A considerable data base for the sedimentary masses on the Australian continent has been developed over past decades by researchers from the Australian National University as a way of estimating the composition of this exposed continental crust (reviewed in Taylor and McLennan, 1985). Special attention has been paid to the Archean and Archean/Proterozoic boundary sedimentary sequences; thus, a fair amount of data exists for samples from the Precambrian Pilbara Block of western Australia (see Fig. 1). A more direct source for Site 765 sediments might be the Phanerozoic rocks of Canning Basin, but these have been ultimately derived from the Archean and Proterozoic blocks of western and central Australia, too (BMR Paleogeographic Group, 1990).

Figures 13A through 13D show Al_2O_3 variation diagrams for Site 765 sediments, along with sediment data from the Canning Basin (Nance and Taylor, 1976), the Pilbara Block (McLennan, 1981; McLennan et al., 1983), and the post-Archean Australian Shale (PAAS) average from Taylor and McLennan (1985). The Pilbara Block sediments include both Archean shales from the George and Whim Creek groups, as well as early Proterozoic sediments from the Hamersley Basin. The Archean shales from the George and Whim Creek groups are too depleted in TiO_2 and Th, and too enriched in Ni and Cr, to be an appropriate source for the Site 765 sediments (Figs. 13A–13D). Furthermore, the Archean shales lack an Eu-anomaly, which is a ubiquitous feature in Site 765 REE patterns (Fig. 10A), and indeed, is the hallmark of post-Archean sediments (Taylor and McLennan, 1985). These characteristics of the George and Whim Creek shales are common to most Archean shales and preclude much of a pure Archean component in the Site 765 sediments. On the other hand, an average of three Canning Basin shales (Paleozoic) provides a good fit with the detrital end-member for Site 765 sediments (Figs. 13A–13D) and makes sense geographically (see Fig. 1) as a source for river or wind influxes to the Exmouth Plateau and Argo Abyssal Plain. The Canning Basin average is near the PAAS composite itself, which is similar to post-Archean shales elsewhere, owing to the remarkable mixing efficiency of sedimentary processes (Taylor and McLennan, 1985). The early Proterozoic Hamersley Basin sediments lie compositionally between the Paleozoic Canning Basin shales and the Archean Pilbara shales, but like the Archean shales, are too Cr-enriched and TiO_2-depleted to be a suitable end-member for Site 765 sediments. Thus, despite significant exposures of Archean rocks in their presumed source, Site 765 sediments are compositionally like post-Archean shales. The ancient age of the source of Site 765 sediments should be reflected, however, in their compositions of Pb and Nd isotopes. Future isotopic work using these samples should help constrain the mean age of the source of Site 765 sediments.

For elements that increase down the hole (e.g., REEs, Fe), the Cenozoic values are more representative of a purely detrital component having a composition near PAAS, which is consistent with the Cenozoic section being dominated by turbidites that quantitatively deliver continental detrital material to the marine environment. The Cretaceous sediments may be enriched over PAAS because of additional hydrogenous, volcanic, hydrothermal, or phosphate contributions, as discussed above.

The proximity of active volcanoes of Java and the Lesser Sunda Islands (Bali, Lombok, Sumbawa, etc.) raises the issue of the extent to which arc andesites contributed to the youngest Site 765 sediments. Ninkovich (1979) demonstrated that Lesser Sunda ash falls extend to only 200 km south of the Sunda Trench. Site 765 lies far south of this zone, and indeed, no prominent ash fall layers were cored in the Cenozoic section. However, it is possible that a disseminated ash component contributed to Site 765 sediments. Figure 14 shows the K_2O and Cr contents of Site 765 sediments, modern Indonesian volcanics, and post-Archean shales. During differentiation of arc magmas, elements incompatible in the fractionating mineral assemblage (such as K) increase dramatically, while compatible elements (Cr) decrease dramatically. Thus, although arc andesites have high K_2O abundances, they are strongly depleted in Cr, unlike marine clays and terrigenous shales that are enriched in both. These systematics apply to the compatible element Ni as well, but Ni may be further enriched in marine sediments from a hydrogenous (Fe-Mn oxide) contribution. The high Cr/K_2O contents throughout the Cenozoic section

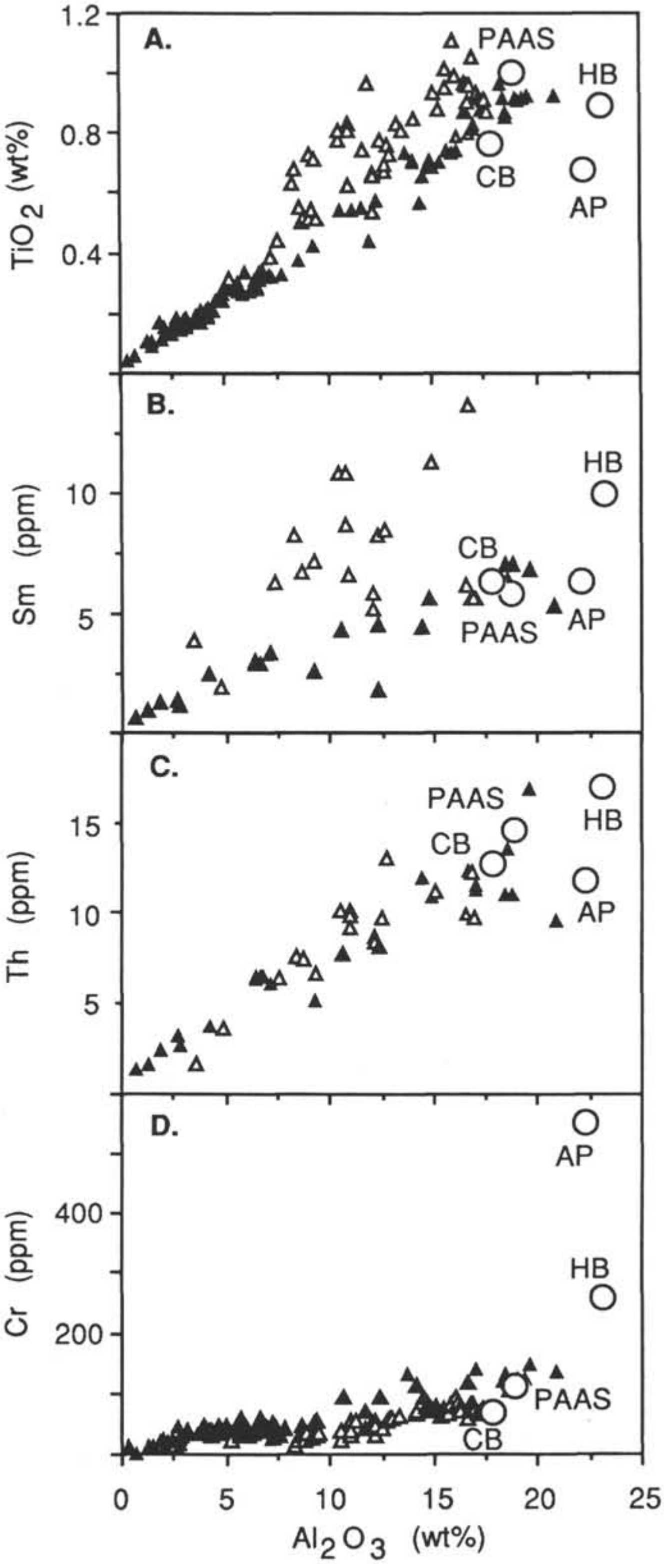

Figure 13. Selected elements vs. Al_2O_3 in Site 765 sediments (open triangles = Cretaceous, closed triangles = Cenozoic), average shales from the Phanerozoic Canning basin (CB), the early Proterozoic Hamersley Basin (HB), and the Archean Pilbara Block (AP), and average post-Archean Australian shale (PAAS). **A.** TiO_2 vs. Al_2O_3. **B.** Sm vs. Al_2O_3. **C.** Th vs. Al_2O_3. **D.** Cr vs. Al_2O_3. Data are from Taylor and McLennan (1985); Nance and Taylor (1976); McLennan et al. (1983); McLennan (1981); and Tables 1 and 2.

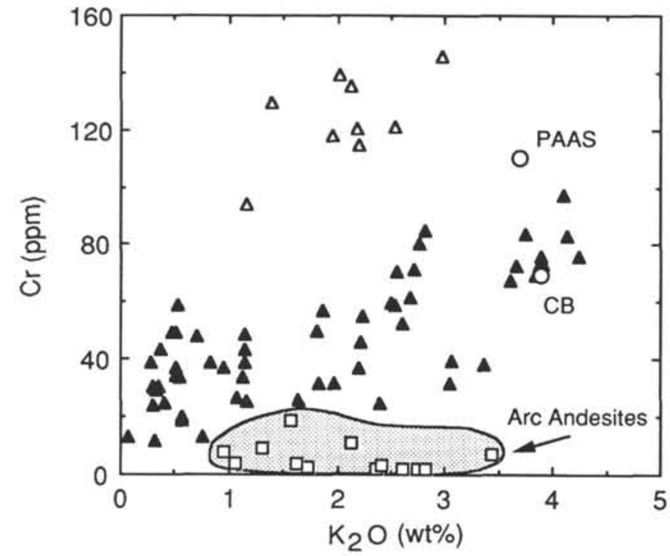

Figure 14. K_2O vs. Cr for Site 765 sediments (triangles), the Canning Basin average and PAAS (as in Fig. 13), and andesites from Java and Lesser Sunda (Merbabu volcano, Java, and Batur volcano, Bali). Data for andesites from Whitford (1975) and Wheller and Varne (1986). Open triangles = anomalously high Cr sediments in the 200- to 400-m interval at Site 765 (Fig. 4B).

rules out much andesitic ash in Site 765 sediments. As Site 765 approaches the Sunda Trench, however, ash may have contributed significantly to the upper sedimentary section, and subduction of this material leads to interesting speculations about the extent of cannibalism at arcs (Ben Othman et al., 1989).

CALCULATING A BULK COMPOSITION FOR SITE 765 SEDIMENTS

Estimating the bulk composition of Site 765 sediments might be as simple as averaging the analyses in Tables 1 and 2. However, this estimate is only as accurate as each sample is representative. Because cc dilution accounts for most of the geochemical variability in Site 765 sediments, this estimate may be refined by taking into account cc variations. Cc contents are linked to macroscopic lithologies (foraminifer sands and nannofossil oozes); thus, published core descriptions provide, in effect, continuous downhole cc estimates. To determine the bulk composition of the site, we estimated the cc content of each 10-m interval (each core) from visual core descriptions, used our analyses to determine the composition of the noncarbonate fraction, and then diluted this composition by the estimated cc content. Details of these calculations are presented next.

The data reported here represent spot analyses that must be weighted by the length of the interval that they represent. For example, some sampled clay units are only centimeters thick, while some sampled nannofossil ooze units are meters long. To determine the weighting factors, the relative proportions of carbonate-rich lithologies were estimated for each of the 103 cores from the barrel sheets in Ludden, Gradstein, et al. (1990). Because a sediment described as "nannofossil ooze" is not pure calcite, shipboard $CaCO_3$ analyses were used to calculate the pure cc fraction for each core. The rest of the core was considered "noncarbonate." Figure 15 presents the downhole variation in this value. This "noncarbonate" factor is simply a way to quantify and smooth lithologic variations downhole. Moreover, because most of the geochemical variability is directly linked to carbonate content, this value links lithologic and geochemical data.

The data in Table 1 were normalized to a carbonate-free, dry basis (by normalizing by a sum that does not include CaO nor the

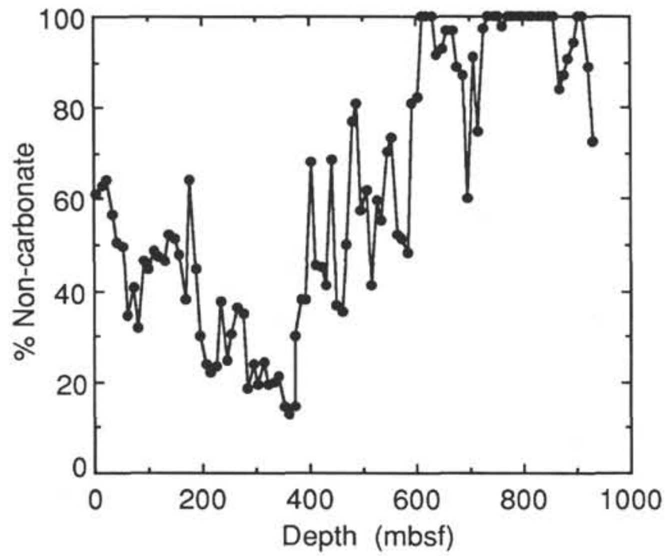

Figure 15. Downhole variation in percentage of noncarbonate per core at Site 765. This value has been estimated from $CaCO_3$ contents and core descriptions in Ludden, Gradstein, et al. (1990). See text for details.

LOI) and averaged for each core. These values were then "diluted" by multiplying by the noncarbonate percentages in Figure 15 to obtain average compositions for each core.

The method of weighting concentrations by the average noncarbonate content is inappropriate for those elements that are contained within carbonate (i.e., Sr), or that do not indicate carbonate dilution relationships (Ba, Mn, P, As, and U). For these elements, individual samples were assumed to be representative of each core. Where more than one analysis per core existed, values were averaged, and where no samples from a core were analyzed, values were interpolated. This method is limited by the extent to which sampling was representative of the dominant lithologies. Because Sr is contained in appreciable amounts in both carbonate (usually >1000 ppm) and clay-rich (usually <200 ppm) units, both clay and carbonate Sr contents were estimated for each core by interpolation of actual measurements, and these values were weighted by the average carbonate content of each core.

Geochemical Logs

These average core compositions provide a smoothed downhole data set that can be compared with geochemical logs. The natural gamma-ray tool (for K, Th, and U), aluminum activation clay tool (for Al), and the gamma-ray spectroscopy tool (for Si, Fe, Ti, and Ca) were run through casing in Hole 765D; the hole was then drilled to set a reentry cone for sampling basement (see also Pratson and Broglia, this volume). Logging through casing decreases the quality of the data because it reduces the signal and adds another factor that must be removed when processing the logs. To smooth these logging data, we applied a five-point running average.

Although logs from the gamma-ray spectroscopy tool proved to have too poor quality to use, the Al_2O_3 and K_2O logs, acquired using two different tools, seem to agree with each other, as well as with the basic lithologic core descriptions. Figure 16 shows K_2O and Al_2O_3 from the logging data for the hole (the upper 170 m was not logged), compared with the weighted averages calculated from our analyses of the core samples. Despite simplification and smoothing of the logging data, the trends agree remarkably well with the "ground truth" analytical data. Both exhibit low values in the 200- to 400-m interval, characterized by low clay content, a peak around 600 m, and lower values deeper in the hole. The average K_2O content of the hole calculated from the logs is 1.5 wt%, while the average calculated from our sediment analyses is 1.6%. The Al_2O_3 log in the interval between 200 and 400 m is about 6 wt% too high, and this may have resulted from a processing artifact, where the highly attenuated signal in this interval may have been overcompensated (Pratson and Broglia, pers. comm., 1990). However, average Al_2O_3 contents calculated for the lower 500 m agree well with the estimate from the weighted core analyses (10.6 vs. 11.1 wt%, from the logs and analyses, respectively).

Bulk Composition of Site 765 Sediments

A grand average for the entire 930-m section was calculated from the core-by-core averages, and this estimate of bulk composition of the hole is presented in Table 4. Separate compositions are presented for the Cenozoic and Cretaceous sections.

Even though significant differences exist between the Cenozoic and Cretaceous sediments, as discussed previously, the primary difference between the two sections is simply their different cc contents. For example, while Sm/Yb increases significantly from 1.9 for the Cenozoic section to 2.4 in the Cretaceous section, Sm concentration itself more than doubles as cc decreases from mean values of 60% to 10%. Thus, dilution is still the dominant signal.

A surprisingly accurate bulk composition for Site 765 sediments may be obtained simply by multiplying an average shale composition (such as PAAS) by the average noncarbonate content of the hole (60%). Table 4 presents the results of these calculations; most elements may be estimated within 30%. Sr can be well approximated by assuming 1500 ppm in the carbonate fraction and PAAS values in the clay fraction. A better fit can be obtained for elements such as K, Nb, Zr, Rb, and Th by taking advantage of their roughly constant and upper crustal-ratios to Al. Along with Al, all these elements are higher in the estimate based simply on PAAS and the carbonate content. By assuming PAAS element/Al_2O_3 ratios and by multiplying by the mean Al_2O_3 content of the Site 765 sediments, better matches for these elements can be obtained. Elements having poor fits include MnO, Cu, and Ni (due to hydrogenous oxides), MgO (due to the diagenetic minerals of the 200- to 400-m interval), Ba (due to radiolarian concentrations) and Cs. Cs/Al_2O_3 is virtually constant in Site 765 sediments, but much lower than PAAS.

The success of the PAAS estimate for most elements suggests that even though extra hydrogenous, volcanic, phosphate, and hydrothermal phases contribute to the Cretaceous sediments, its composition is still dominated by average shales. By assuming an average shale composition (PAAS), a relatively accurate estimate of the bulk composition of the hole can be made without relying on any chemical analyses: the carbonate dilution factor can be estimated from visual core descriptions, and average Al or K contents, which constrain crustal ratios, can be determined from geochemical logs.

SITE 765 AS A REFERENCE SECTION

Marine sediments are largely mixtures of four components: biogenic, detrital, hydrogenous, and hydrothermal (Dymond, 1981; Leinan, 1987). The hydrothermal component is only important near an active ridge-crest hydrothermal system, although disseminated components may be far reaching (1000 km, Barrett, 1987). The hydrogenous component, associated with Fe-Mn oxides, dominates only when the other components are absent, such as is typical for the South Pacific, much of which is below the CCD and far removed from regions of high biologic productivity and terrigenous sources. Site 765 represents the other end-member. Near a continental margin, the site is dominated by biogenic

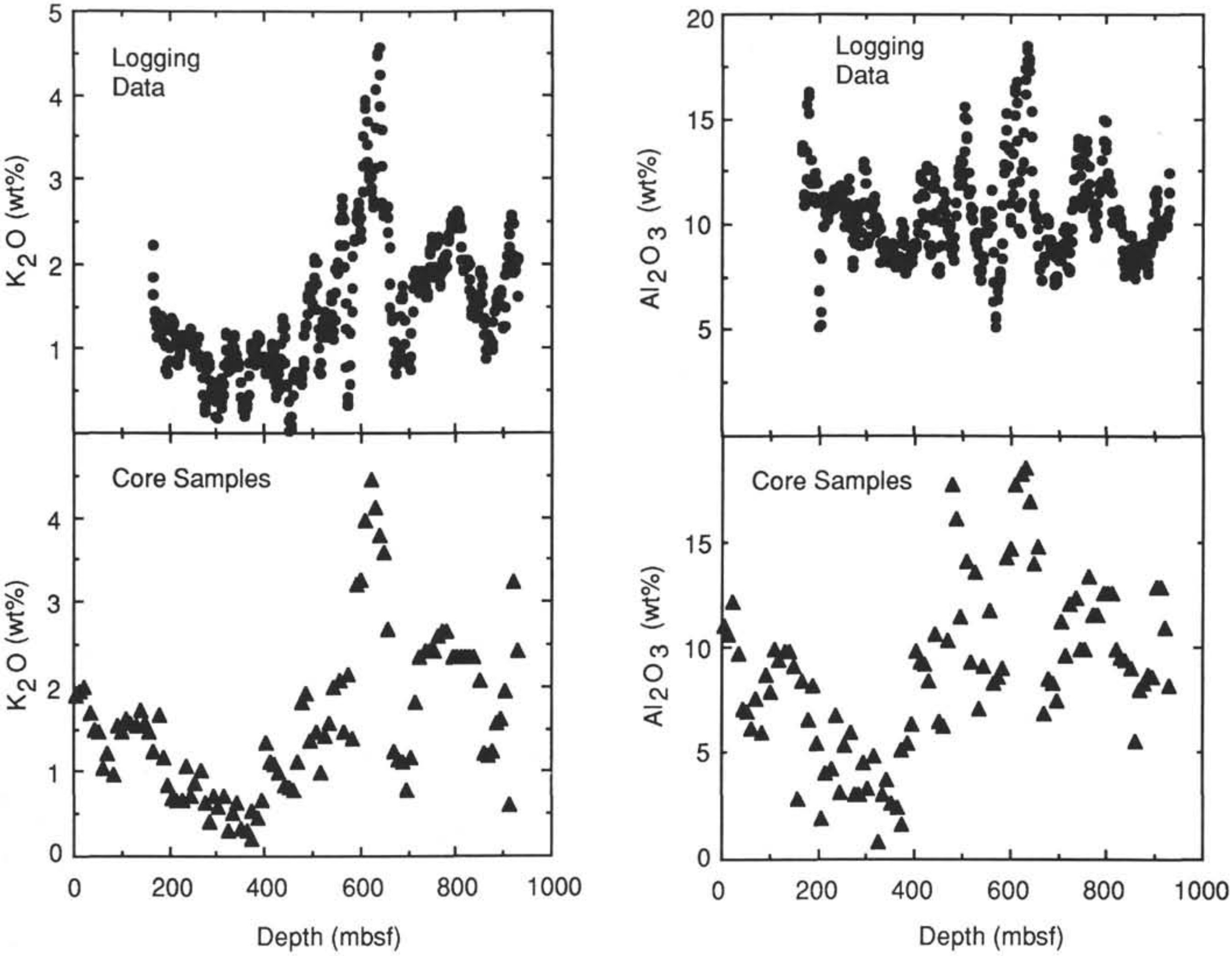

Figure 16. Downhole logs for K_2O and Al_2O_3 (from Pratson and Broglia, this volume) compared with weighted analyses of core samples. See text for details of weighting and data processing. Downhole K_2O variations from the two methods agree remarkably well. Al_2O_3 content agrees well in sediments below 400 mbsf.

and detrital material. This leads directly to the success of the simple calculation based on PAAS and cc content to describe the bulk composition of Site 765. The large biogenic influx means that variations in the other components are overwhelmed by simple quantitative dilution. However, proximity to a continent also means that the detrital component is relatively constant as well, owing to the remarkable homogeneity of mature upper crustal material. Indeed, McLennan et al. (1990), in a survey of deep-sea turbidites, found that passive margin turbidites typically sample average, old, upper crustal material. These two factors, dilution because of biogenic components and average crustal detritus, should make calculating sedimentary columns adjacent to continents elsewhere just as simple. Results from Site 765 suggest that accurate estimates may be made with little analytical effort. Continental margin sections exist outboard of other arcs than Indonesia (the Antilles, Chile, Alaska, Cascades, Mediterranean) and thus make up a significant portion of potentially subducted material. In contrast, sedimentary sections in the middle of the Pacific, such as outboard of the Tonga Arc, have been starved of biogenic and detrital components and may require a completely different way to calculate bulk compositions. Future research will be dedicated to establishing another reference section in the central South Pacific.

Although much of the variation in a sedimentary section proximal to a continental margin will reduce simply to dilution of average crustal shales by biogenic material, this still leads to some interesting systematics for elements that are important tracers of crustal recycling:

1. Alkali elements (K, Rb, Cs). These elements are entirely coupled to the detrital component and will be quantitatively diluted by biogenic material. Their ratios may be similar to average crustal shales, although K may vary with clay mineralogy (Fig. 6). Deeply weathered source regions may contribute more kaolinite-rich clays, leading to lower K/Al than average shales. McLennan et al. (1990) also suggested that the alkali elements may fractionate from each other during weathering, with low K/Cs contents characteristic of highly weathered sources.

2. Alkaline earth elements (Sr, Ba). In contrast, these elements have little to do with the detrital component, and thus important fractionations in alkali/alkaline earth elements occur in the marine environment. Sr substitutes for Ca in marine carbonates and may be present in concentrations up to 3000 ppm in some aragonites. Nonetheless, we have shown that the average Sr content of a sedimentary section such as that at Site 765 can be well estimated simply by assuming average cc and shale values. Although Ba

Table 4. Bulk composition of Site 765 sediments.

	Site 765 Ceno	Site 765 Cret	Whole Hole	PAAS	Calc 765	Calc from Al	% diff
SiO_2	26.8	65.6	42.5	64.2	39.66		-7
TiO_2	.37	.70	.50	1.02	.63	.47	-7
Al_2O_3	7.4	11.2	8.9	19.3	11.93	8.90	0
FeO	2.8	6.0	4.1	6.6	4.10		0
MnO	.11	.46	.25	.11	.07		-73
MgO	2.9	2.6	2.7	2.2	1.39		-49
CaO	32.2	5.5	21.4	1.3	21.39	(from cc)	0
Na_2O	.9	1.4	1.1	1.2	.76		-30
K_2O	1.3	2.2	1.6	3.8	2.34	1.74	6
P_2O_5	.13	.14	.14	.16	.10		-26
total cc	57.5	9.8	38.2				
Nb	5.4	10.4	7.4	19.4	12.0	8.9	21
Zr	93	125	106	215	133	99	-7
Y	17	29	21	28	17		-20
Sr	1285	274	871	204	699	(from cc)	-20
Rb	48	72	58	163	101	75	31
Zn	56	95	72	87	54		-25
Cu	71	197	122	51	32		-74
Ni	42	71	54	56	35		-35
Cr	53	45	50	112	69	52	4
V	66	112	85	153	95		12
Ba	319	1913	963	664	410		-57
Sc	7.2	13.8	9.9	16	10	8	-24
La	17	36	24	39	24		-2
Ce	31	93	56	82	51		-10
Nd	13	31	20	33	20		-1
Sm	2.8	7.0	4.5	5.72	3.54		-22
Eu	.59	1.44	.94	1.12	.69		-26
Tb	.41	.91	.61	.79	.49		-21
Yb	1.5	2.9	2.1	2.86	1.77		-14
Lu	.24	.46	.33	.44	.27		-17
Cs	3.3	4.3	3.7	15.3	9.5	7.1	90
Hf	2.7	3.8	3.1	5.1	3.2	2.4	-25
Ta*	.41	.74	.67				
W*	2.3	4.0	3.5				
Co*	9	27	21	23.5	14.5		-30
As	4.3	8.0	5.8				
Sb	.9	.7	.9				
Th	5.8	8.9	7.0	14.9	9.2	6.9	-2
U	1.8	.9	1.5	3.2	2.0		31

* Samples powdered in WC excluded from estimate for these elements.
PAAS from Taylor and McLennan (1985), renormalized to 100%.

exhibits complex behavior in the marine environment, Ba contents may be enormously high (10,000 ppm levels) in siliceous oozes. A rough association exists between Ba and radiolarian abundances in Site 765 sediments (Figs. 3B and 3C). This association may result from barite nucleation on decaying siliceous skeletons in the water column (Bishop, 1988). Predominance of siliceous organisms is a characteristic of regions of high productivity maintained by active upwelling, such as in equatorial regions. Thus, Ba has been used as a paleoproductivity indicator, as well as an equatorial reference frame for charting plate motions (Schmitz, 1987).

3. REEs. The REEs typically display post-Archean shale patterns and are quantitatively diluted by cc and silica. REEs may become enriched, however, by phosphate or Fe-Mn oxide phases. Positive Ce anomalies are characteristic of sediments rich in Fe-Mn oxides, while negative Ce anomalies are characteristic of sediments rich in biogenic cc or phosphate. A few arc volcanics possess negative Ce anomalies (Heming and Rankin, 1979), which might have been inherited from REE-rich phosphates.

4. High field-strength elements (HFSE; Nb, Ta, Hf, Zr). These elements, like the alkalis, are completely coupled to the detrital component, although they may become enriched in turbidite sands from heavy mineral concentrations. The high concentrations of HFSE in sediments and the notoriously low concentrations in arc volcanics provide convincing evidence against *bulk* assimilation of sediment in subduction zones. The transfer of material from the subducting slab to the asthenosphere beneath arcs must be one selective to certain elements (Morris and Hart, 1983).

5. Parent/daughter ratios. Although carbonate dilution has had a dramatic effect on *concentrations* of elements, the *ratios* of several elements remain relatively constant throughout Site 765 sediments, especially in the Cenozoic sequence. Indeed, we took advantage of the constant and upper crustal ratios for several elements to refine our estimate of the bulk composition of Site 765 sediments. For example, the Sm/Nd ratio is remarkably constant in Site 765 sediments, even though Sm concentrations may vary by a factor of 20 because of cc dilution. Important radioactive parent/daughter ratios, however, will vary significantly with carbonate content. The most obvious is Rb/Sr, which decreases significantly in carbonate-rich lithologies as a result of both dilution of Rb and incorporation of Sr in marine carbonates. The U/Th ratio will vary in an inverse way, because Th is quantitatively diluted, while U is somewhat taken up in carbonates (Ben Othman et al., 1989). Thus, first-order variations in these important parent-daughter ratios may also be controlled by carbonate content.

SEDIMENT SUBDUCTION ALONG THE SUNDA TRENCH

Although not the specific aim of this study, these data for Site 765 sediments have obvious applications to sediment recycling at the Sunda Arc. Geophysical observations along the Sunda Trench are ambiguous regarding structural evidence for sediment subduction. A large gradient in sediment thickness occurs along the Sunda Trench (Fig. 17). In the northwest, south of Sumatra, there may be as much as 5 km of sediment, much of which is being accreted in the forearc (Moore et al., 1980). Farther east, south of Java, only a thin veneer of sediment approaches the trench: as little as 200 m in places (Moore et al., 1980). Available seismic data, however, show little resolvable structure within the Java Trench slope and thus leave open the question of sediment accretion (Curray et al., 1977).

The isotope ^{10}Be was measured in samples from 10 volcanoes on Java and on Bali, and abundances were indistinguishable from lavas in other tectonic settings (Tera et al., 1986). A lack of ^{10}Be enrichment in Indonesian volcanics does not prove that sediments were not subducted beneath Java. Because ^{10}Be has such a short half-life (about 1.5 m.y.), it is present only in Neogene sediments, and the absence of ^{10}Be in Java volcanics might simply mean that Neogene sediments were not subducted and erupted within 10 m.y. (the time over which ^{10}Be decays). It is entirely possible that older sediments are being subducted. Whitford and Jezek (1982) suggested that sediments were incorporated in the source of Java magmas, based on the radiogenic Pb isotopic compositions and steep $^{207}Pb/^{204}Pb$ vs. $^{206}Pb/^{204}Pb$ trend defined by Java volcanics. These data have long served as one of the classic examples for sediment incorporation, even though no sediment data were available at the time Whitford and Jezek (1982) formed their model. However, new Pb isotopic data for piston core samples of sediments outboard of Java overlap with the volcanics (Ben Othman et al., 1989) and provide new support for the original interpretation. Thus, the most compelling argument for subduction comes from Pb isotopic data.

Some data exist with which to extrapolate the lithologic and geochemical stratigraphies developed at Site 765 regionally along the Sunda Arc. Several holes that penetrated basement were drilled during DSDP Legs 22 and 27, and although recovery was poor (often less than 20%), data from these holes do provide a means of estimating the lithologic sections around the Sunda Trench (see Fig. 17). These holes include two around the Australian margin (Sites 261 and 260), two farther west in the Wharton Basin (Sites 212 and 213), and one just south of the Sunda Trench (Site 211). From descriptions in the Initial Reports volumes of these cruises, it appears that calcareous turbidites from the Australian margin extend as far north as Site 261 and as far west as Site 212 in the Wharton Basin. Site 213 contains little carbonate, but has accumulated siliceous oozes since the Miocene. An extensive section of Site 211 is composed of clastic turbidites of the Nicobar Fan.

A small amount of geochemical data has been published for sediments from Sites 261 and 260 (largely major elements; Cook, 1974), Sites 211 through 213 (transition metals; Pimm, 1974), and for a few piston cores outboard of the Sunda Trench (trace elements and isotopes; Ben Othman et al., 1989; see Fig. 17). Because no shared set of elements exists, one finds it difficult to draw many regional conclusions. Future research will include isotopic

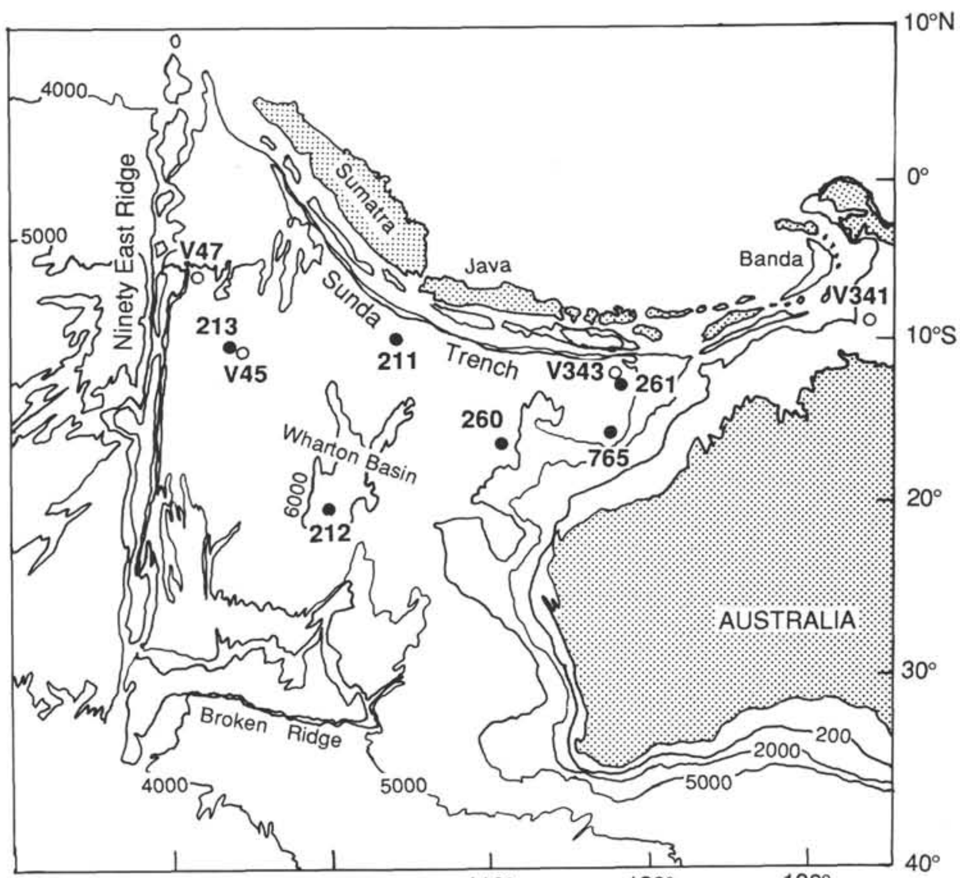

Figure 17. Location map of other DSDP and ODP holes (closed circles) throughout the region outboard of the Sunda Trench. Water depth in meters. Open circles are piston cores V34-47, V34-45, V28-341, and V28-343 from Ben Othman et al. (1989) that are discussed in the text (other piston cores from Ben Othman et al., 1989, are on the north side of the Sunda Trench and are not discussed here).

analyses of Site 765 sediments, as well as analyses of major and trace elements in the piston core samples for which Ben Othman et al. (1989) analyzed isotopes. These data will allow for more confident extrapolation of information along the entire Sunda Arc. However, the following preliminary observations can be made. Sites 260 and 261 along the Australian margin are similar to Site 765 in that the Cretaceous section is dominated by clays, the Cenozoic section contains calcareous turbidites, and the detrital end-member, at least based on the K_2O/TiO_2 ratios (Fig. 18), appears similar to PAAS. Although one would wish to analyze more clay samples for more elements, calculating the bulk composition of these two sites may be as simple as estimating the cc and Al contents, as we demonstrated for Site 765 sediments.

MnO-rich clays may be more common from the Wharton Basin sites than from those sites nearer the Australian margin (Fig. 19).

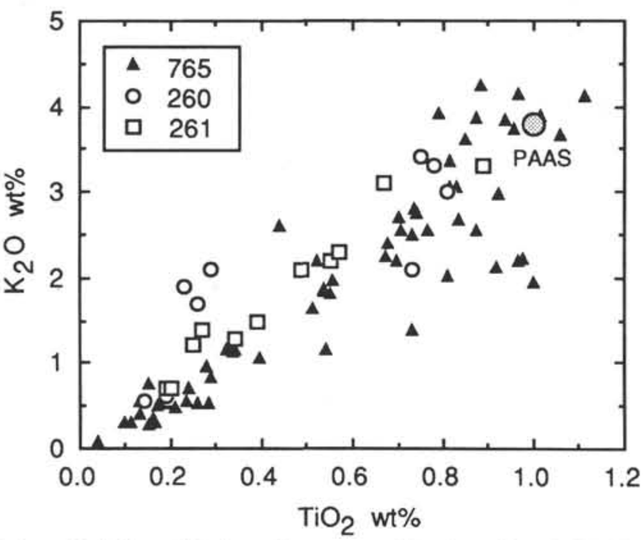

Figure 18. K_2O vs. TiO_2 for sediments around the Argo Abyssal Plain. Data for DSDP Sites 260 and 261 from Cook (1974).

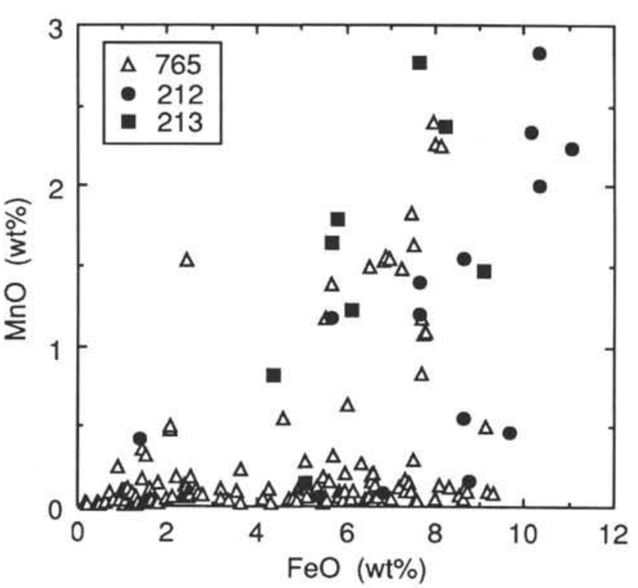

Figure 19. FeO* vs. MnO for sediments from DSDP Sites 212 and 213 in or near the Wharton Basin and Site 765. Data for Sites 212 and 213 from Pimm (1974).

Although no higher in concentration than the most manganiferous sediments from Site 765, almost all of the samples analyzed from Sites 212 and 213 are rich in MnO, perhaps reflecting a greater hydrogenous/detrital fraction in the clays. This interpretation is consistent with these sections being farther from the Australian continent and their detrital sources. The isotopic compositions of the piston core samples near the Australian margin are distinctive of old cratonic material (i.e., high $^{207}Pb/^{204}Pb$, low $^{143}Nd/^{144}Nd$), while those west of the Wharton Basin are distinctly less enriched (Fig. 20), perhaps reflecting influx of younger material from the Nicobar Fan. The Wharton Basin sample has higher Lu contents than any sample from Site 765, while other piston core samples as far west as the Ninetyeast Ridge and as far east as the Banda Islands overlap completely with Site 765 sediments (Fig. 21).

Existing data are patchy, but suggest it may be possible to extrapolate at least certain aspects of Site 765 sediments across the entire basin from the Banda Islands to Ninetyeast Ridge. Australian continental detritus is most likely an important component of sediments at least out into the Wharton Basin. Key analyses of other important components, such as Mn-rich clays of the Wharton Basin, clastic material fed from the Nicobar Fan, and ash from the active arc, coupled with careful consideration of the lithologic characteristics of the DSDP holes (e.g., carbonate vs. clay fractions), might yield good first-order estimates of elemental fluxes into the Sunda Trench.

CONCLUSIONS

1. The dominant signal in the geochemical variability of Site 765 sediments is dilution of a detrital component by biogenic calcium carbonate and silica. This dilution leads to enormous variations in the concentrations of most elements. Dilution from carbonate or silica may be a long-lived feature of the sedimentary column, even if subducted to great depths because of the relatively high temperatures required for decarbonation reactions (Gill, 1981; Abbott and Lyle, 1984).

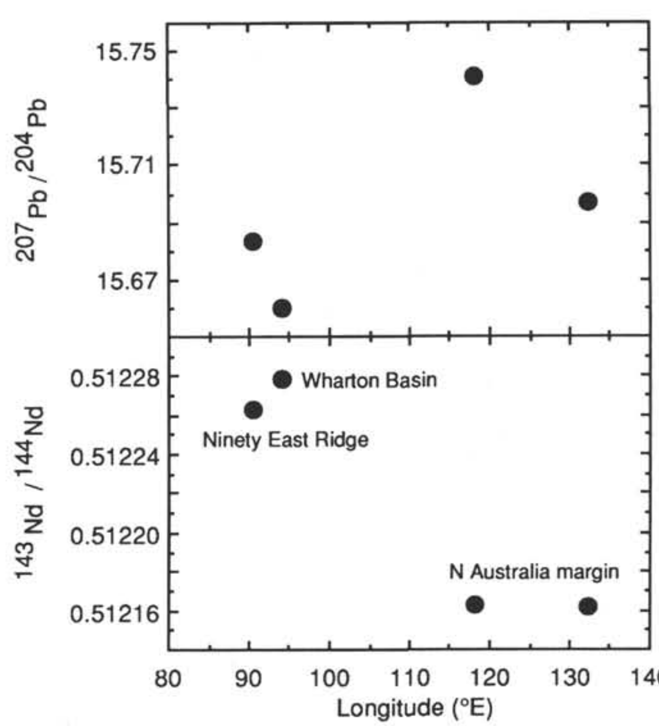

Figure 20. Pb and Nd isotopic compositions for surface samples outboard of the Sunda Trench (from Ben Othman et al., 1989).

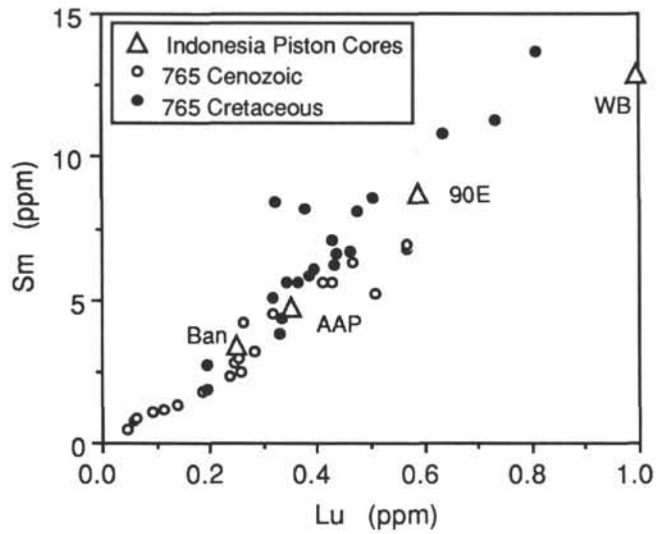

Figure 21. Sm and Lu concentrations for Site 765 sediments and the four piston core samples shown in Figure 20 from the Banda region (BAN), Argo Abyssal Plain (AAP), Ninetyeast Ridge (90E), and Wharton Basin (WB).

2. Significant differences occur between Cenozoic and Cretaceous clays, involving increases in Fe, Ti, Mn, Ba, REEs, changes in REE patterns, and development of positive Ce anomalies down the section. These variations may result from increases in hydrogenous, hydrothermal, phosphate, and/or volcanic phases during the Cretaceous. Although important for identifying changes in the provenance, sediment supply, or rate with time, these phases led to small deviations from the average composition of the hole, which is dominated by dilution of an average shale composition.

3. The K_2O and Al_2O_3 downhole logs correspond well with "ground truth" chemical analyses. The bulk composition of the hole can be calculated by using the visual core descriptions to weight the individual analyses over appropriate intervals. This composition, however, agrees remarkably well (to 30% for most elements) with an estimate based simply on average Australian shales and the average cc and Al_2O_3 contents of the hole. This result suggests that estimating other sections dominated by carbonate and continental detritus may require minimal analytical effort. Ideally, only core descriptions and logging data should provide estimates of cc and Al contents that are accurate enough to characterize a site.

4. Although Site 765 is an important reference section for sedimentary columns along the Sunda Arc, our results are more general. Site 765 sediments are well described by dilution of average shale by biogenic phases, and because average shale compositions are remarkably similar around the world, results from Site 765 are general, not restricted to provenances or processes about the Indonesian region. Site 765 should thus serve as a useful reference for calculating other continental margin sections approaching trenches around the world (e.g., the Antilles, Americas, Mediterranean). A recent study by Hay et al. (1988) about global distribution of sediments on the ocean floor estimated that roughly 40% of ocean sediments is calcium carbonate and roughly 45% is terrigenous detrital material. Therefore, Site 765 sediments, dominated by cc and terrigenous detritus, is representative of a large part of the global marine sedimentary reservoir.

ACKNOWLEDGMENTS

We thank Ginger Eberhart, Gilles Gauthier, and Bettina Domeyer for technical assistance with the DCP, INAA, and XRF analyses, respectively. Scott McLennan kindly provided unpublished data and a preprint. We thank Charlie Langmuir for helpful discussions and support, and S. M. McLennan and C. R. Czerna for useful reviews. Mitch Lyle and John Compton are especially appreciated for making themselves available for an onslaught of questions. T. Plank gratefully acknowledges financial support from USSAC and from a JOI/USSAC Graduate Fellowship.

REFERENCES

Abbott, D., and Lyle, M., 1984. Age of oceanic plates at subduction and volatile recycling. *Geophys. Res. Lett.,* 11:951–954.

Aplin, A. C., 1984. Rare earth element geochemistry of Central Pacific ferromanganese encrustations. *Earth Planet. Sci. Lett.,* 71:13–22.

Barrett, T., Taylor, P. N., and Lugowski, J., 1987. Metalliferous sediments from DSDP Leg 92: the East Pacific Rise transect. *Geochim. Cosmochim. Acta,* 51:2241–2253.

Ben Othman, D., White, W. M., and Patchett, J., 1989. The geochemistry of marine sediments, island arc magma genesis and crust-mantle recycling. *Earth Planet. Sci. Lett.,* 94:1–21.

Bishop, J.K.B., 1988. The barite-opal organic carbon association in oceanic particulate matter. *Nature,* 332:341–343.

BMR Paleogeographic Group, 1990. *Australia: Evolution of a Continent:* Canberra (Australian Govt. Publ. Serv.).

Cook, P. J., 1974. Major and trace element geochemistry of sediments from DSDP, Leg 27, Sites 259–263, eastern Indian Ocean. *In* Veevers, J. J., Heirtzler, J. R., et al., *Init. Repts. DSDP,* 27: Washington (U.S. Govt. Printing Office), 481–498.

Curray, J. R., Shor, G. G., Raitt, R. W., and Henry, M., 1977. Seismic refraction and reflection studies of crustal structure of the Eastern Sunda and Western Banda arcs. *J. Geophys. Res.,* 82:2479–2489.

Dymond, J., 1981. The geochemistry of Nazca Plate sediments: an evaluation of hydrothermal, biogenic, detrital, and hydrogenous sources. *In* Kulm, L. D., Dymond, J., Dasch, D. M., and Hussong, D. M. (Eds.), *Nazca Plate: Crustal Formation and Andean Convergence.* Geol. Soc. Am. Mem., 154:133–174.

Elderfield, H., and Greaves, M. J., 1981. Negative cerium anomalies in the rare earth element patterns of oceanic ferromanganese nodules. *Earth Planet. Sci. Lett.,* 55:163–170.

Elderfield, H., and Pagett, R., 1986. Rare earth elements in ichtyholiths: variations with redox conditions and depositional environment. *Sci. Total Environ.,* 49:175–197.

Francis, D., and Ludden, J. N., 1990. The mantle source for olivine nephelinite, basanite and alkali olivine basalt at Fort Selkirk, Yukon, Canada. *J. Petrol.,* 31:371–400.

Gill, J. B., 1981. *Orogenic Andesites and Plate Tectonics:* New York (Springer-Verlag).

Govindaraju, K., 1989. 1989 compilation of working values and sample description for 272 geostandards. Spec. Iss. Geostds. Newsl., 13:1–113.

Hay, W. M., Sloan, J. L., and Wold, C. N., 1988. Mass/age distribution and composition of sediments on the ocean floor and the global rate of sediment subduction. *J. Geophys. Res.,* 93:14933–14940.

Heming, R. F., and Rankin, P. C., 1979. Ce-anomalous lavas from Rabaul caldera, Papua New Guinea. Geochim. Cosmochim. Acta, 43:1351–1355.

Hussong, D. M., Uyeda, S., et al., 1981. *Init. Repts. DSDP,* 60: Washington (U.S. Govt. Printing Office).

Karig, D. E., and Kay, R. W., 1981. Fate of sediments on the descending plate at convergent margins. *Philos. Trans. R. Soc. London,* 301:233–251.

Klein, E. M., Langmuir, C. H., and Staudigel, H. S., 1991. Geochemistry of basalts from the SE Indian Ridge, 115°–138°. *J. Geophys. Res.,* 96:2089–2108.

Leinen, M., 1987. The origin of paleochemical signatures in North Pacific pelagic clays: partitioning experiments. *Geochim. Cosmochim. Acta,* 51:305–319.

Ludden, J. N., Gradstein, F. M., et al., 1990. *Proc. ODP, Init. Repts.,* 123: College Station, TX (Ocean Drilling Program).

McLennan, S. M., 1981. Trace element geochemistry of sedimentary rocks: implications for the composition and evolution of the continental crust [Ph.D. dissert.]. Australian National Univ., Canberra.

McLennan, S. M., Taylor, S. R., and Eriksson, K. A., 1983. Geochemistry of Archean shales from the Pilbara Supergroup, Western Australia. *Geochim. Cosmochim. Acta,* 47:1211–1222.
McLennan, S. M., Taylor, S. R., McCulloch, M. T., and Maynard, J. B., 1990. Geochemical and Nd-Sr isotopic composition of deep-sea turbidites: crustal evolution and plate tectonic associations. *Geochim. Cosmochim. Acta,* 54:2015–2050.
Moore, G. F., Curray, J. R., Moore, D. G., and Karig, D. E., 1980. Variations in geologic structure along the Sunda fore arc, northeastern Indian Ocean. *In* Hayes, D. E. (Ed.), *The Tectonic and Geologic Evolution of Southeast Asian Seas and Islands.* Am. Geophys. Union, 145–160.
Morris, J. D., and Hart, S. R., 1983. Isotopic and incompatible element constraints on the genesis of island arc volcanics from Cold Bay and Amak islands, Aleutians, and implications for mantle structure. *Geochim. Cosmochim. Acta,* 47:2015–2030.
Nance, W. B., and Taylor, S. R., 1976. Rare earth element patterns and crustal evolution. I. Australian post-Archean sedimentary rocks. *Geochim. Cosmochim. Acta,* 40:1539–1551.
Ninkovich, D., 1979. Distribution, age and chemical composition of tephra layers in deep-sea sediments off western Indonesia. *J. Volcanol. Geotherm. Res.,* 5:67–86.
Palmer, M. R., 1985. Rare earth elements in foraminifera tests. *Earth Planet. Sci. Lett.,* 73:285–298.
Pimm, A. C., 1974. Mineralization and trace element variaitons in deep-sea pelagic sediments of the Wharton basin, Indian Ocean. *In* von der Borch, C. C., Sclater, J. G., et al., *Init. Repts. DSDP,* 22: Washington (U.S. Govt. Printing Office), 469–476.
Schmitz, B., 1987. Barium, equatorial high productivity, and the northward wandering of the Indian continent. *Paleoceanography,* 2:63–77.
Schweller, W. J., Kulm, L. D., and Prince, R. A., 1981. Tectonics, structure, and sedimentary framework of the Peru-Chile Trench. *Mem. Geol. Soc. Am.,* 154:323–349.
Staudigel, H., Doyle, P., and Zindler, A., 1985. Sr and Nd isotopic systematics in fish teeth. *Earth Planet. Sci. Lett.,* 76:45–46.
Taylor, S. R., and Gorton, M. P., 1977. Geochemical application of spark source mass spectrometry. III. Element sensitivity, precision and accuracy. *Geochim. Cosmochim. Acta,* 41:1375–1380.
Taylor, S. R., and McLennan, S. M., 1985. *The Continental Crust: Its Composition and Evolution:* Oxford (Blackwell Scientific).
Tera, F., Brown, L., Morris, J., Sacks, I. S., Klein, J., and Middleton, R., 1986. Sediment incorporation in island-arc magmas: inferences from 10Be. *Geochim. Cosmochim. Acta,* 50:535–550.
Toyoda, K., Nakamura, Y., and Masuda, A., 1990. Rare earth elements of Pacific pelagic sediments. *Geochim. Cosmochim. Acta,* 54:1093–1103.
von Huene, R., 1986. To accrete or not to accrete, that is the question. *Geol. Rundsch.,* 75:1–15.
Warsi, W.E.K., Hilde, T.W.C., and Searle, R. C., 1983. Convergence structures of the Peru Trench between 10°S and 14°S. *In* Hilde, T.W.C., and Uyeda, S. (Eds.), *Convergence and Subduction.* Tectonophysics, 99:313–329.
Watkins, J. S., Moore, J. C., et al., 1982. *Init. Repts. DSDP,* 66: Washington (U.S. Govt. Printing Office).
Westbrook, G. K., Ladd, J. W., Buhl, P., Bangs, N., and Tiley, G. J., 1988. Cross section of an accretionary wedge: Barbados Ridge complex. *Geology,* 16:631–635.
Wheller, G. E., and Varne, R., 1986. Genesis of dacitic magmatism at Batur volcano, Bali, Indonesia: implications for origins of stratovolcano calderas. *J. Volcanol. Geotherm. Res.,* 28:363–378.
Whitford, D. J., 1975. Geochemistry and petrology of volcanic rocks from the Sunda arc, Indonesia [Ph.D. dissert.]. Australian National Univ., Canberra.
Whitford, D. J., and Jezek, P. A., 1982. Isotopic constraints on the role of subducted sialic material in Indonesian island-arc magmatism. *Geol. Soc. Am. Bull.,* 93:504–513.

Date of initial receipt: 19 July 1990
Date of acceptance: 16 August 1991
Ms 123B-158